




Snail-regulated exosomal microRNA-21 suppresses NLRP3 inflammasome activity to enhance cisplatin resistance

Han-Ying Cheng ¹, Chia-Hsin Hsieh,² Po-Han Lin ^{1,3}, Yu-Tung Chen,¹ Dennis Shin-Shian Hsu,⁴ Shyh-Kuan Tai,⁵ Pen-Yuan Chu,⁵ Muh-Hwa Yang ^{1,2,3,6}

To cite: Cheng H-Y, Hsieh C-H, Lin P-H, *et al.* Snail-regulated exosomal microRNA-21 suppresses NLRP3 inflammasome activity to enhance cisplatin resistance. *Journal for ImmunoTherapy of Cancer* 2022;**10**:e004832. doi:10.1136/jitc-2022-004832

► Additional supplemental material is published online only. To view, please visit the journal online (<http://dx.doi.org/10.1136/jitc-2022-004832>).

Accepted 05 August 2022



© Author(s) (or their employer(s)) 2022. Re-use permitted under CC BY-NC. No commercial re-use. See rights and permissions. Published by BMJ.

¹Institute of Clinical Medicine, National Yang Ming Chiao Tung University, Taipei, Taiwan

²Institute of Biotechnology and Laboratory Science in Medicine, National Yang Ming Chiao Tung University, Taipei, Taiwan

³Cancer Progression Research Center, National Yang Ming Chiao Tung University, Taipei, Taiwan

⁴Asclepiumm Taiwan Co., Ltd, Taipei, Taiwan

⁵Department of Otolaryngology, Taipei Veterans General Hospital, Taipei, Taiwan

⁶Division of Medical Oncology, Department of Oncology, Taipei Veterans General Hospital, Taipei, Taiwan

Correspondence to

Professor Muh-Hwa Yang; mhyang2@nycu.edu.tw

ABSTRACT

Background Compared with the precise targeting of drug-resistant mutant cancer cells, strategies for eliminating non-genetic adaptation-mediated resistance are limited. The pros and cons of the existence of inflammasomes in cancer have been reported. Nevertheless, the dynamic response of inflammasomes to therapies should be addressed.

Methods Tumor-derived exosomes were purified by differential ultracentrifugation and validated by nanoparticle tracking analysis and transmission electron microscopy. A proximity ligation assay and interleukin-1 β (IL-1 β) level were used for detecting activation of NLRP3 inflammasomes. RNA sequencing was used to analyze the exosomal RNAs. *MIR21* knocked out human monocytic THP cells and *mir21* knocked out murine oral cancer MTCQ1 cells were generated for confirming the exosomal delivery of microRNA (miR)-21. Syngeneic murine models for head and neck cancer (C57BL/6J), breast cancer (BALB/C) and lung cancer (C57BL/6J) were applied for examining the impact of Snail-miR21 axis on inflammasome activation in vivo. Single-cell RNA sequencing was used for analyzing the tumor-infiltrated immune cells. Head and neck patient samples were used for validating the findings in clinical samples.

Results We demonstrated that in cancer cells undergoing Snail-induced epithelial-mesenchymal transition (EMT), tumor cells suppress NLRP3 inflammasome activities of tumor-associated macrophages (TAMs) in response to chemotherapy through the delivery of exosomal miR-21. Mechanistically, miR-21 represses *PTEN* and *BRCC3* to facilitate NLRP3 phosphorylation and lysine-63 ubiquitination, inhibiting NLRP3 inflammasome assembly. Furthermore, the Snail-miR-21 axis shapes the post-chemotherapy tumor microenvironment (TME) by repopulating TAMs and by activating CD8⁺ T cells. In patients with head and neck cancer, the Snail-high cases lacked post-chemotherapy IL-1 β surge and were correlated with a worse response.

Conclusions This finding reveals the mechanism of EMT-mediated resistance beyond cancer stemness through modulation of post-treatment inflammasome activity. It also highlights the dynamic remodeling of the TME throughout metastatic evolution.

INTRODUCTION

The emergence of therapeutic resistance during cancer progression is a major obstacle in combating advanced cancers. The reasons

WHAT IS ALREADY KNOWN ON THIS TOPIC

⇒ Therapeutic resistance emerges during late-stage progression of cancers.

WHAT THIS STUDY ADDS

⇒ The epithelial-mesenchymal transition-undergoing cancer cells deliver microRNA-21-abundant exosomes to suppress inflammasome activities of macrophages for enhancing resistance.

HOW THIS STUDY MIGHT AFFECT RESEARCH, PRACTICE OR POLICY

⇒ A dynamic interplay between cancer and microenvironments indicates the importance of real-time adjustment of therapeutic strategies alongside cancer progression.

for the acquired resistance of malignant tumors include the genetic evolution of cancer cells and non-genetic adaptation to therapies.¹ The non-genetic plasticity of cancer cells enables lineage switching to adapt to the environment and facilitates the evasion of anticancer immunosurveillance. Compared with the rapid advances in sequencing techniques and precise targeting of resistant mutants, strategies for eliminating non-genetic adaptation-mediated resistance are relatively limited.

The dynamic switch between epithelial and mesenchymal states is crucial for cancer metastasis and therapeutic resistance.² In addition to the well-established impact of epithelial-mesenchymal transition (EMT) on cancer stemness and therapeutic resistance,³ accumulated evidence, including findings reported by our previous studies, supports the bidirectional interaction between EMT-undergoing cancer cells and host immune cells.^{4–7} EMT is well known for both engendering immunosuppression^{8–10} and for promoting the creation of proinflammatory tumor microenvironments (TMEs).^{5 11 12} Compared with the well-established role of

EMT reported in tumor immunosuppression, the impact of EMT on the modulation of the response of host innate immune cells in response to stimuli/treatments is less clear.

Inflammasomes, the multimolecular complexes that consist of an NOD-like receptor scaffold, caspase activation, adapter proteins such as ASC (also known as Pycard), and caspase-1, are considered major sensors of innate immunity which function in response to danger signals in mammals.¹³ Although chronic inflammation has been noted as a critical event in tumorigenesis and cancer progression, the contradictory roles of inflammasomes in the TME have been demonstrated in different contexts. The pro-cancer and anticancer effects of inflammasomes have both been reported.^{14–17} Diverse stimuli such as ATP, bacterial components, or nucleic acids induce the assembly of inflammasomes, leading to caspase-1 activation and secretion of interleukin-1 β (IL-1 β) and IL-18.¹³ Post-treatment dying cancer cells release danger signals, such as nucleic acids, high-mobility group box 1 (HMGB1) protein, and ATP, which trigger innate immunity and inflammation.^{18–20} However, knowledge about the impact of the post-therapeutic activation of inflammasomes on treatment response is relatively limited.

The present study demonstrated that in cancers undergoing Snail-induced EMT, tumor cells suppressed the activity of inflammasomes of tumor-associated macrophages (TAMs) in response to chemotherapy through the delivery of exosomal microRNA (miR)-21. The miR-21 modulates NLRP3 phosphorylation and lysine 63-ubiquitination to inhibit the assembly of NLRP3 inflammasomes, thereby shaping the post-chemotherapy TME and reducing the chemotherapy response. This finding reveals the mechanism of EMT-mediated therapeutic resistance beyond cancer stemness through modulation of post-treatment inflammasome activities. It also highlights the dynamic remodeling of the TME throughout metastatic evolution.

MATERIALS AND METHODS

Cell lines and plasmids

Human head and neck squamous cell carcinoma (HNSCC) cell line FaDu, human monocytic leukemia cell line THP-1, human embryonic kidney cell line 293T, BALB/c mouse breast carcinoma cell line 4T1, and C57BL/6J mouse lung carcinoma cell line LLC1 were originally sourced from the American Type Culture Collection. The HNSCC cell line OECM-1 and the C57BL/6J murine oral cancer cell line MTCQ1 were kindly provided by Dr Kuo-Wei Chang (National Yang Ming Chiao Tung University of Taiwan). The pCDH-Snail, pCDH-Zeb1 and pCDH-MIR21 plasmids were generated via insertion of full-length cDNA (SNAIL: NM_005985; ZEB1: NM_030751.4, MIR21: NR_029493.1) into the pCDH-CMV-MCS-EF1-puro vector. The pcDNA3-Flag-NLRP3 plasmid was provided by Dr Szu-Ting Chen (National Yang Ming Chiao Tung University of

Taiwan). The 3'-untranslated region (UTR) of *BRCC3* (NM_001018055) was cloned into pMIR-REPORTER to generate pMIR-BRCC3-wt, and site-directed mutagenesis was performed to generate the miR-21 binding-site-mutated pMIR-BRCC3-mut.

Patient with HNSCC samples

Five independent sets of samples were used for the experiments. The informed consent was obtained from all patients in this study. The information of the patient samples is detailed in online supplemental methods and online supplemental tables 1-5.

Single-cell RNA-sequencing

To obtain cells for single-cell RNA-sequencing (scRNA-seq) analysis, 1×10^6 MTCQ1-WT/MTCQ1^{mir21-/-} cells were inoculated into the subcutaneous region of C57BL/6 mice. Cisplatin (5 mg/kg) was administered intraperitoneally on the 14th day, and tumors were harvested on the 17th day. Tumors were dissociated using a tumor dissociation kit (Miltenyi Biotec), and dead cells were removed using a dead cell removal kit (MACS). CD45⁺ tumor-infiltrating immune cells were isolated using microbeads (Miltenyi Biotec). Cell viability detected via trypan blue staining was over 85% for subsequent sequencing. For library construction and sequencing, we used the droplet-based scRNA-seq (10x Genomics Chromium Single Cell 3' Reagent Kit V.3.1, no. 1000121) for single-cell library preparation. After the conduction of reverse transcription, complementary DNA sequencing was performed using the Illumina NovaSeq 6000 (Illumina). The quality control (QC) and filtering steps were performed using a loupe browser. Briefly, data on cells with low total counts and high mitochondrial gene expression were filtered. The scRNA-seq reads were processed using a 10x Genomics Cell Ranger pipeline and analyzed using the Partek Flow software (Partek, St. Louis, Missouri, USA). Clustering of cells in our dataset was performed using a t-distributed stochastic neighbor embedding (t-SNE) algorithm in Partek Flow. To identify the t-SNE subclusters present in different types of immune cells, the average gene expression of each cluster was identified using cluster identity predictor (CIPR).²¹ Gene Ontology (GO) analysis of the differentially expressed genes between clusters was performed using DAVID²² and GSEA.²³ Partek Flow was used for gene-specific analysis, macrophage re-clustering, macrophage trajectory analysis, and volcano plot generation.

Data and code availability

The accession numbers for the data reported in this paper are GEO: GSE99474, GSE172326, GSE178537, and GSE 181300.

Statistical analysis

Statistical analyses were performed using GraphPad Prism V.8 (GraphPad Software). Two-sided independent Student's t-test (normal distribution) Pearson's correlation test was used to analyze the correlation between the

two continuous factors. All statistical data were derived from at least three independent biological replicates, and each experiment contained at least two technical replicates. P value ≤ 0.05 was considered statistically significant (*: ≤ 0.05 , **: ≤ 0.01 , ***: ≤ 0.001).

RNA-seq analysis of patient with HNSCC samples, RNA-seq for exosomal small RNA, preparation of conditional media and macrophages, purification and characterization of tumor-derived exosomes, tissue processing and data generation for Visium spatial gene expression, generation of the *MIR21/mir21* knockout cell lines, quantitative real-time PCR, immunoblotting and immunoprecipitation, immunohistochemistry, multiplex immunofluorescence staining of HNSCC samples, proximity ligation assay, luciferase reporter assay, SYTOX green assay, and animal experiments: The information of the experiments is detailed in online supplemental methods.

RESULTS

Supernatants derived from Snail-expressing cancer cells suppress the NLRP3 inflammasome activity

In the present study, we considered HNSCC as the major model for experiments based on the crucial role of EMT reported in HNSCC progression and on our previous findings reported in HNSCC EMT studies.^{24–25} Since Snail has been identified as the major EMT regulator affecting microenvironments, we performed multiplex immunofluorescence staining to examine the immune cells in HNSCC samples with different expression levels of Snail. A noticeable increase in the infiltration of CD163⁺ TAMs was observed in samples with higher Snail expression (online supplemental figure 1A and online supplemental table 1). Next, we analyzed the correlation between EMT and inflammatory cytokines in the RNA-seq data of HNSCC samples retrieved from The Cancer Genome Atlas (TCGA) and the cohort of Taipei Veterans General Hospital (TVGH) (figure 1A–B and online supplemental table 2). The samples were categorized as EMT^{high} or EMT^{low} according to the calculated EMT score,²⁶ and a higher expression of transforming growth factor β (TGF- β) validated the feasibility of the categorization. Increased expression of cytokines related to cancer progression and immunosuppression, such as IL-6, tumor necrosis factor (TNF- α) (in the TCGA cohort), and IL-10 (in both cohorts), was observed in the EMT^{high} group, which was consistent with previous reports.^{4, 27–28} Intriguingly, a trend of reduced levels of IL-1 β (in the TCGA cohort) or IL-18 (in the TVGH cohort) was noted in the EMT^{high} group, indicating the potential influence of EMT on inflammasome activity. We further applied spatial transcriptomic technology in a HNSCC sample to validate the relationship between EMT and inflammasome activation. A trend of a reversed relationship between the gene expression profile of EMT and inflammasome-related genes was shown (online supplemental figure 1C), (online supplemental table 6), indicating the potential of EMT in suppression of inflammasome activity in HNSCC.

We have previously shown that Snail-expressing cancer cells recruit TAMs through the secretion of CCL2, CCL5, and TNF- α to facilitate cancer progression.⁴ Snail-expressing cancer cells secrete exosomes to promote M2 polarization of TAMs.⁶ We examined the influence of Snail on inflammasome activity. Snail was overexpressed in FaDu, a human HNSCC cell line harboring low-endogenous Snail (left panel of figure 1C). Snail knockdown was performed in the high-endogenous Snail human HNSCC cell line OECM1⁴ (left panel of figure 1D). The supernatant derived from FaDu-Snail inhibited the release of active caspase-1 and IL-1 β from activated peripheral blood mononuclear cells (PBMC)-derived macrophages compared with the control cells (figure 1C). Knockdown of Snail in OECM1 potentiated the release of active caspase-1 and IL-1 β (figure 1D). Consistent results were observed in the human monocytic cell line THP1-derived activated macrophages. Supernatants from FaDu-Snail repressed IL-1 β secretion from THP1-derived activated macrophages. Supernatants from OECM1-Snail knockdown cells did not potentiate the secretion of IL-1 β to a significant level (online supplemental figure 2A). In contrast, the supernatant derived from FaDu cells expressing another major EMT regulator, Twist1, did not affect the secretion of active caspase-1 and IL-1 β from THP1-derived activated macrophages (online supplemental figure 2B).

We further confirmed the effect of Snail-expressing cancer cells on NLRP3 inflammasome assembly. When the NLRP3 inflammasome is activated, NLRP3 establishes interactions with ASC to recruit and activate caspase-1. Concurrently, the complexes are assembled into a giant pyroptosome. Proximity ligation assay (PLA) was performed to examine the interaction between NLRP3 and ASC in PBMC-derived and THP1-derived macrophages. The supernatant derived from FaDu-Snail repressed the interaction between NLRP3 and ASC in activated macrophages compared with the control cells (figure 1E and online supplemental figure 2C). The FaDu-Snail supernatant also reduced pyroptosome formation in activated macrophages (figure 1F). As chemotherapy reportedly activates the NLRP3 inflammasome,^{14, 20} we examined whether Snail-overexpressing cancer cells suppressed chemotherapy-activated inflammasomes in macrophages. Cisplatin treatment activated inflammasomes in macrophages as expected, and FaDu-Snail supernatant suppressed the activity of inflammasomes, as evidenced by the reduction of active caspase-1 and IL-1 β production (online supplemental figure 2D). The FaDu-Snail supernatant also reduced the NLRP3-ASC interaction in cisplatin-activated macrophages (figure 1G). Altogether, the above-mentioned results indicate that the supernatant derived from FaDu-expressing HNSCC suppresses NLRP3 inflammasome activity.

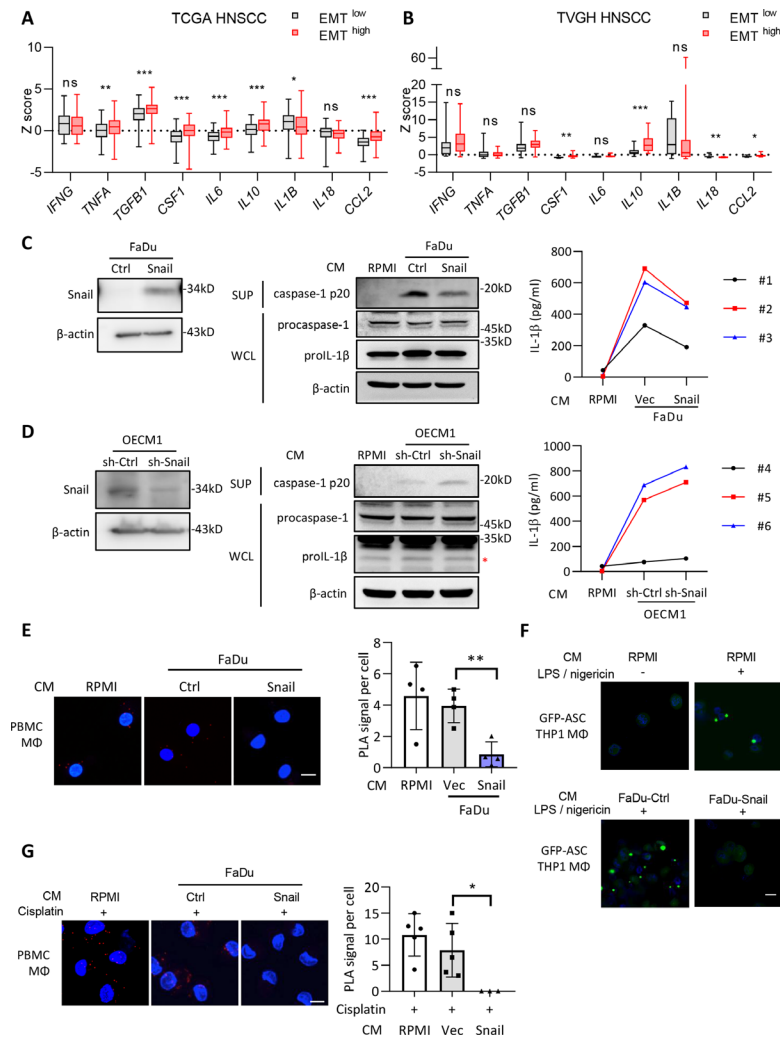


Figure 1 The supernatants of Snail-expressing cancer cells inhibit activation of NLRP3 inflammasomes. (A–B) Analysis of the expression of the inflammation-related genes in the TCGA HNSCC database (A) or Taipei Veterans General Hospital (TVGH) database. The samples were categorized as the EMT^{high} and EMT^{low} group according to the expression of the EMT-related genes (*VIM*, *FN1*, *CDH2*, *ITGB6*, *FOXC2*, *MMP2*, *MMP3*, *MMP9*, *SOX10*, *SNAI1*, *SNAI2*, *TWIST1*, *GSC*, *CDH1*, *DSP*, *TJP1*) (see Chae *et al.*)²⁶ n=521 for TCGA, n=65 for TVGH. The boxplots show the minimum, first quartile, medium, third quartile, and maximum. *p<0.05, **p<0.01, ***p<0.001, ns=no significance by Student's t-test. (C) Left, western blot of Snail in FaDu-Ctrl/Snail. β-actin was a loading control. Middle, immunoblots of cleaved caspase-1 p20 in supernatants (SUP), pro-caspase-1 and pro-IL-1β in whole cell lysates (WCL) of PBMC-derived macrophages cultivated in conditioned media (CM) from FaDu cells stably transfected with Snail or a control vector (Ctrl) for 48 hours. RPMI was a control for CM. β-actin was a loading control for immunoblots of WCL. Right, ELISA for analyzing the level of secreted IL-1β from PBMC-derived macrophages cultivated with the conditional media from FaDu-Snail/FaDu-Vec. Peripheral blood mononuclear cells were isolated from three different healthy donors (case #1, #2, and #3). (D) Left, western blot of Snail in OECM1-sh-Ctrl/sh-Snail. β-actin was a loading control. Middle, immunoblots of cleaved caspase-1 p20 in SUP, pro-caspase-1 and pro-IL-1β in WCL of PBMC-derived macrophages cultivated in CM from OECM1 cells receiving short hairpin RNA against Snail (sh-Snail) or a control sequence (sh-Ctrl) for 48 hours. RPMI was a control for CM. β-actin was a loading control for immunoblots of WCL. Right, ELISA for analyzing the level of secreted IL-1β from macrophages cultivated with the conditional media from FaDu-Snail/FaDu-Vec. Peripheral blood mononuclear cells were isolated from three different healthy donors (case #4, #5, and #6). (E) Left, representative images of proximity ligation assay (PLA) for detecting NLRP3 and ASC interaction in PBMC-derived macrophages cultivated in CM from FaDu-Vec or FaDu-Snail. The red dots indicate the PLA signals. Scale bar, 10 μm. Right, quantification of number of PLA signals per cell. For each group, at least a total of 18 cells from four randomly selected fields were used for PLA quantification. Data represent means±SD. **p<0.01 by Student's t-test. (F) Representative immunofluorescent images of THP1-derived macrophages transfected with GFP-tagged ASC, stimulated with nigericin and cultivated with the CM from FaDu-Ctrl, FaDu-Snail, or RPMI for 24 hours. Scale bar, 10 μm. (G) PLA for detecting NLRP3 and ASC interaction in cisplatin-activated PBMC-derived macrophages incubated with CM from FaDu-Vec/FaDu-Snail. Left, representative images. Red dots indicate PLA signals. Scale bar, 10 μm. Right, quantification of PLA signals per cell. For each group, at least total 16 cells from five random selections (three for FaDu-Snail) were used for PLA quantification. Data represent means±SD. *p<0.05 by Student's t-test. Scale bar, 10 μm. EMT, epithelial-mesenchymal transition; HNSCC, head and neck squamous cell carcinoma; IL, interleukin; PBMC, peripheral blood mononuclear cells; TCGA, The Cancer Genome Atlas.

Snail-expressing cancer cells suppress NLRP3 inflammasome activity through the secretion of miR-21-abundant exosomes

Next, we determined the major player(s) in the suppression of inflammasome activity in the supernatant of Snail-expressing cancer cells. We found that IL-6, IL-8, CCL2, and CCL5 were the major cytokines regulated by Snail.^{4,29} However, neutralization of these cytokines did not affect NLRP3-ASC interaction or pyroptosome formation in activated macrophages subjected to treatment with the supernatant derived from either FaDu-Snail or control cells (online supplemental figure 3A-B). As tumor-secreted exosomes (TEXs) have been critically involved in remodeling microenvironments,^{30,31} we investigated whether Snail-expressing cancer cell-secreted exosomes modulated the inflammasome activity in macrophages. The exosomes were confirmed via direct visualization by performing transmission electron microscopy and nanoparticle tracking analysis, and results showed the presence of 50–150 nm nanovesicles with bilayer membranes (online supplemental figure 3C). The markers of exosomes, including CD9, CD63, CD81, and Alix, were examined to confirm the successful purification of cancer-secreted exosomes (online supplemental figure 3D). We investigated the effect of TEXs on the inflammasome activity of macrophages. A significant reduction in the NLRP3-ASC interaction was noted when activated macrophages were subjected to treatment with FaDu-Snail-secreted exosomes compared with those derived from FaDu-control cells (figure 2A). Consistently, a decrease in IL-1 β secretion was also noted when macrophages were incubated with FaDu Snail-secreted exosomes (figure 2B). These data indicate that Snail-expressing cell-secreted exosomes suppress the activity of the NLRP3 inflammasome in activated macrophages.

MicroRNAs (miRNAs) are important components of regulatory networks in innate immunity.³² We have previously shown that *MIR21* transcription was regulated by Snail, and miR-21-abundant exosomes secreted from Snail-overexpressing HNSCC promote M2-like polarization of TAMs.⁶ We hypothesized that exosomal miRNAs might provide a link between cancer cells and innate immune signaling pathways. To this end, we performed exosomal miRNA sequencing in the human HNSCC cell line FaDu versus immortalized human gingival mucosa cells SG. We investigated the miRNAs that were especially enriched in TEXs, the tumor-specific exosomal miRNAs, by focusing on the top 10 miRNAs in FaDu-derived exosomes. Among them, miR-21 was found to be the most significantly enriched in the TEXs (online supplemental table 7). As EMT is closely linked to miRNA dysregulation,³³ and as Snail dominates the expression of several miRNAs in cancer cell,^{34,35} we explored the major Snail-regulated exosomal miRNA(s) by examining the expression of the top-ranked tumor exosomal miRNAs in FaDu-Snail versus FaDu-control and OECM1 that received a short hairpin RNA (shRNA) against Snail or a control

sequence. Among these, miR-21, miR-10a, and miR-191 showed consistency in upregulated levels of FaDu-Snail-secreted exosomes and downregulated levels of exosomes derived from the Snail-knockdown OECM1 cells (online supplemental figure 4A). We further examined the impact of the three miRNAs on NLRP3 inflammasome activation. Transfection of miR-21, but not miR-10a/miR-191, into THP1-derived macrophages significantly attenuated the interaction between NLRP3 and ASC (online supplemental figure 4B). Consistently, miR-21 reduced the assembly of NLRP3 and ASC (figure 2C) and IL-1 β secretion in PBMC-derived macrophages (figure 2D). Together with our previous finding which highlighted that Snail upregulated exosomal miR-21 levels through direct or indirect (via Zeb1) activation of *MIR21* transcription,⁶ the results indicated the potential involvement of Snail-regulated miR-21 in the suppression of NLRP3 inflammasome activity.

To further elucidate the role of exosomal miR-21 in the regulation of NLRP3 inflammasome activity in macrophages, we generated *MIR21* knockout THP1 cells using the CRISPR-Cas9 technology (online supplemental figure 4C). A significant increase in IL-1 β secretion was noted in the supernatant of THP1^{*MIR21*^{-/-}}-derived macrophages subjected to treatment with LPS and nigericin compared with the wild-type THP1-derived macrophages (figure 2E). Knockout of miR-21 in THP1 increased NLRP3-ASC interaction in THP1-derived macrophages (figure 2F). Treatment of THP1^{*MIR21*^{-/-}}-derived macrophages with exosomes harvested from miR-21-overexpressed FaDu cells reduced NLRP3-ASC interaction (figure 2G). To further confirm the role of Snail-regulated miR-21 in the suppression of inflammasome activity, we knocked down miR-21 in Snail-overexpressing FaDu cells (FaDu-Snail) and examined the impact of the TEXs on IL-1 β secretion of macrophages. The efficacy of the miRZip anti-miR-21 was validated by the reporter assay (online supplemental figure 4D). Downregulation of miR-21 reporter activity was shown in Snail-overexpressing FaDu cells, and the successful knockdown of miR-21 was confirmed by the restoration of reporter activity in FaDu-Snail transfected with anti-miR-21 (online supplemental figure 4E). We next examined the impact of the Snail-miR-21 axis in cancer cells on the inflammasome activity of macrophages through delivering exosomes. The macrophages were treated with TEXs derived from FaDu-control, FaDu-Snail, and FaDu-Snail-anti-miR21. Overexpression of Snail in FaDu cells suppressed IL-1 β secretion of macrophages, and knockdown of miR-21 in FaDu-Snail restored the IL-1 β level (figure 2G). Consistently, overexpression of Snail in FaDu cells reduced NLRP3-ASC interaction (detected by PLA) and knockdown of miR-21 in FaDu-Snail restored the interaction (figure 2H). In summary, these results indicate that exosomal miR-21 from Snail-overexpressing cancer cells attenuates NLRP3 inflammasome activation of macrophages.

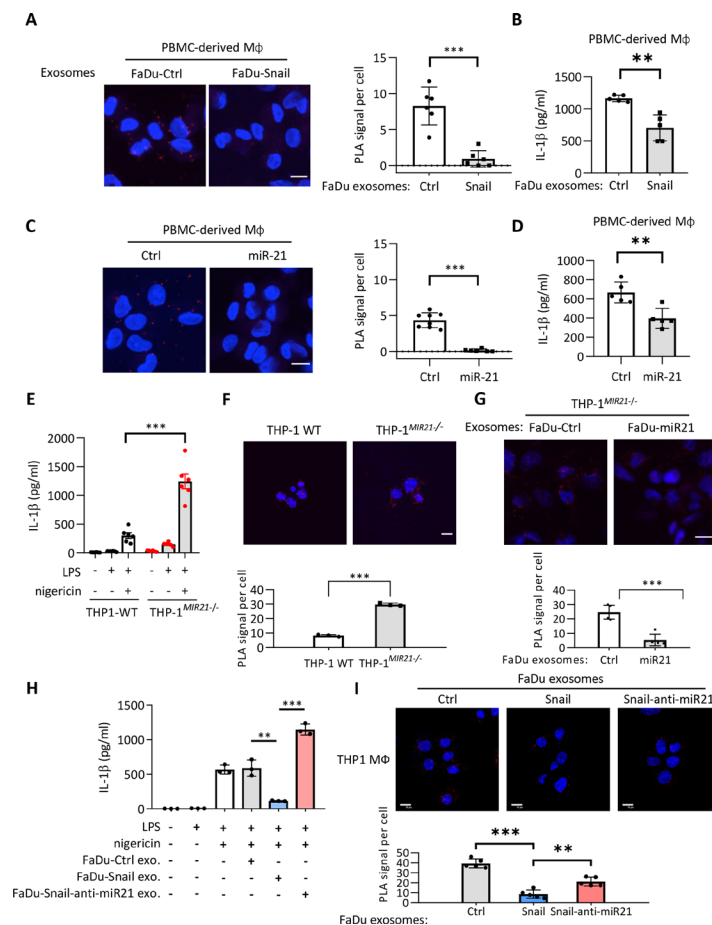


Figure 2 Exosomes from Snail-miR-21 axis activated cancer cells suppress NLRP3 inflammasome activity of macrophages. (A) Representative images of PLA for detecting NLRP3 and ASC interaction in PBMC-derived macrophages incubated with the exosomes from FaDu-Vec/FaDu-Snail. The red dots indicate the PLA signals. Scale bar, 10 μ m. Right, quantification of number of PLA signals per cell. For each group, at least a total of 50 cells from six randomly-selected fields were used for PLA quantification. Data represent means \pm SD. *** p <0.001 by Student's t-test. (B) ELISA for analyzing the level of secreted IL-1 β by PBMC-derived macrophages incubated with exosomes from FaDu-Vec/FaDu-Snail. n =5 independent experiments (each experiment contains two technical replicates). Data represent means \pm SD. ** p <0.01 by Student's t-test. (C) Left, representative images of PLA for detecting NLRP3 and ASC interaction in PBMC-derived macrophages transduced with miR-21 or a control agomir. The red dots indicate the PLA signals. Scale bar, 10 μ m. Right, quantification of number of PLA signals per cell. For each group, at least a total of 60 cells from randomly-selected fields (six for miR-21 group and eight for ctrl group) were used for PLA quantification. Data represent means \pm SD. *** p <0.001 by Student's t-test. (D) IL-1 β ELISA of PBMC-derived macrophage. miR-21 agomir or a control sequence (Ctrl) was transduced to macrophage. n =5 independent experiments (each experiment contains two technical replicates). Data represent means \pm SD. ** p <0.01 by Student's t-test. (E) ELISA for analyzing the level of secreted IL-1 β by macrophages derived from wild-type THP1 (THP1-WT) or *MIR21*-knockout THP1 (THP1^{MIR21-/-}). The macrophages were treated with/without LPS (1 μ g/mL) and nigericin (5 μ M). n =6 (each contains two technical replicates) for each group. Data represent means \pm SD. *** p <0.001 by Student's t-test. (F) Representative images of PLA for detecting NLRP3 and ASC interaction in THP1-WT/THP1^{MIR21-/-}-derived activated macrophages. The red dots indicate the PLA signals. Scale bar, 10 μ m. Right, quantification of number of PLA signals per cell. For each group, at least a total of 400 cells from five randomly selected fields were used for PLA quantification. Data represent means \pm SD. *** p <0.001 by Student's t-test. (G) Representative images of PLA for detecting NLRP3 and ASC interaction in THP1^{MIR21-/-}-derived macrophages incubated with exosomes from FaDu cells transfected with miR-21-expressing vector (FaDu-miR21) or a control vector (FaDu-Ctrl). The red dots indicate the PLA signals. Scale bar, 10 μ m. For each group, at least a total of 400 cells from five randomly selected fields were used for PLA quantification. Data represent means \pm SD. *** p <0.001 by Student's t-test. (H) ELISA for analyzing the level of secreted IL-1 β by THP1-derived macrophages. The macrophages were treated with/without LPS (1 μ g/mL) and nigericin (5 μ M) and the exosomes from FaDu cells transfected with a control vector (FaDu-ctrl), Snail-expressing vector (FaDu-Snail), Snail and anti-miR-21 (FaDu-Snail-anti-miR21). n =3 (each contains two technical replicates) for each group. Data represent means \pm SD. ** p <0.01, *** p <0.001 by Student's t-test. (I) Representative images of PLA for detecting NLRP3 and ASC interaction in THP1^{MIR21-/-}-derived activated macrophages incubated with exosomes from FaDu cells transfected with a control vector, a miR-21-expressing vector, or Snail together with an antagonist for miR-21 (Snail-anti-miR21). The red dots indicate the PLA signals. Scale bar, 10 μ m. For each group, at least a total of 400 cells from five randomly selected fields were used for PLA quantification. Data represent means \pm SD. ** p <0.01, *** p <0.001 by Student's t-test. IL, interleukin; miR, micro RNA; PBMC, peripheral blood mononuclear cells; PLA, proximity ligation assay.

miR-21 modulates NLRP3 phosphorylation and polyubiquitination to suppress inflammasome activity

We next investigated the mechanism of miR-21-mediated suppression of NLRP3 inflammasome activity. Neither miR-21 agomir nor the miR-21-abundant exosomes (harvested from Snail-expressing cancer cells) affected the messenger RNA (mRNA) levels of *NLRP3/ASC* (online supplemental figure 5A) or the protein stability of NLRP3/ASC (online supplemental figure 5B). Knockout of miR-21 did not downregulate the expression of A20, a negative regulator of nuclear factor kappa B (NF- κ B),³⁶ in LPS/nigericin-stimulated THP1 cells (online supplemental figure 5C). Therefore, we considered that miR-21 repressed inflammasome activity by reducing the interaction between NLRP3 and ASC. Transfection with miR-21 reduced the interaction between NLRP3 and ASC (figure 3A; see also figure 2C). Post-translational modifications of NLRP3, including phosphorylation and K63-ubiquitination, are reportedly crucial for the assembly of NLRP3 inflammasomes for subsequent activation.^{20 37 38}

Next, we investigated the mechanisms responsible for the miR-21-regulated NLRP3 inflammasome activation. Regarding phosphorylation-regulated NLRP3 inflammasome activities, PTEN has been shown to dephosphorylate tyrosine 32 of NLRP3 to facilitate NLRP3 inflammasome activation.²⁰ PTEN has been observed to be a direct target suppressed by miR-21.³⁹ Here, we showed that knockout of *MIR21* in THP-1 cells upregulated *PTEN* (figure 3B) and reduced NLRP3 phosphorylation (figure 3C). In addition to phosphorylation, polyubiquitination of NLRP3 is critical in the regulation of inflammasome activity. Furthermore, NLRP3 is the substrate of BRCA1/BRCA2-containing complex subunit 3 (BRCC3), a deubiquitinase that specifically cleaves lysine 63-linked polyubiquitin chains.³⁸ Intriguingly, *BRCC3* contains the seed regions of miR-21 predicted by using TargetScan, and the sequences of the seed regions are preserved across species (online supplemental figure 5D), indicating the potential for miR-21-mediated inflammasome inactivation by targeting *BRCC3*. Ectopic expression of miR-21 in PBMC-derived macrophages downregulated *BRCC3* expression (online supplemental figure 5E). Increased BRCC3 protein and mRNA expression levels were noted in the *MIR21* knockout subline of THP1 cells (figure 3D). Co-incubation of activated macrophages with the supernatants derived from FaDu-Snail versus FaDu-control cells showed that the FaDu-Snail supernatant upregulated miR-21 expression and downregulated the expression levels of *PDCD4* (a known target of miR-21) and *BRCC3* in macrophages (online supplemental figure 5F). A consistent result was observed in OECM1 cells that received shRNA against Snail versus a control sequence. The supernatants derived from Snail-knockdown OECM1 cells reduced miR-21 and increased *BRCC3* and *PDCD4* expression (online supplemental figure 5G). The reporter containing the wild-type or mutated miR-21 binding sites of *BRCC3* 3'-UTR was generated to investigate the regulation of *BRCC3* by miR-21 (online supplemental figure

5H). Ectopic miR-21 suppressed the wild-type *BRCC3* reporter, whereas mutation of the miR-21 binding motifs abrogated this effect (figure 3E).

We examined whether miR-21 inhibited NLRP3 inflammasome activation by suppressing NLRP3 deubiquitination. NLRP3 was immunoprecipitated from HEK293T cells co-transfected with NLRP3 and K63 ubiquitin plus miR-21/control vector. Overexpression of miR-21 increased the level of K63 ubiquitination of NLRP3 (figure 3F). Stable expression of miR-21 inhibited the deubiquitination of NLRP3 in THP-1 cells stimulated with nigericin (figure 3G). Reduced K63 ubiquitination was observed in macrophages derived from THP-1^{MIR21-/-} cells compared with wild-type THP1 cells (figure 3H). Together, these results indicate that miR-21 or miR-21-abundant exosomes from Snail-expressing cells suppress NLRP3 inflammasome activity by targeting *PTEN* to enrich tyrosine phosphorylation of NLRP3, and by targeting *BRCC3* to enhance K63 ubiquitination of NLRP3.

Snail and miR-21 inhibit chemotherapy-induced NLRP3 inflammasome activation and attenuate chemotherapy responses in vivo

NLRP3 inflammasome-produced active caspase-1 and IL-1 β are necessary for chemotherapy-induced anti-tumor immunity.¹⁴ We hypothesized that Snail-regulated miR-21 reduced activation of the NLRP3 inflammasome of macrophages which attenuates chemotherapy-induced anti-tumor immunity of cancer cells, which contributed to the development of chemotherapy resistance. To this end, we used three syngeneic murine tumor models for the experiments. We first investigated the role of tumorous miR-21 in chemotherapy response in a syngeneic murine HNSCC model⁴⁰ (the oral squamous cell carcinoma cell line MTCQ1 derived from C57B6/J mice) and generated the *mir21* knockout murine HNSCC cell line MTCQ1^{mir21-/-} (figure 4A). We inoculated wild-type and *mir21* knockout MTCQ1 cells into the subcutaneous region of wild-type C57B6/J mice to enable the formation of syngeneic HNSCC tumors, following which treatments were conducted with cisplatin. Tumors were harvested 4 days after treatment to assess caspase-1 activity to indicate inflammasome activity (figure 4B). Cisplatin treatment increased caspase-1 activity of F4/80⁺ TAMs from wild-type MTCQ1 tumors, whereas knockout of *mir21* significantly enhanced caspase-1 activation in TAMs (figure 4C; the gating strategy of caspase 1-positive cells is illustrated in online supplemental figure 6A). To investigate the impact of miR-21-regulated Nlrp3 inflammasomes on chemotherapy responses, we inoculated the wild-type murine MTCQ1 cells or MTCQ1^{mir21-/-} cells to the wild-type or *Nbp3*^{-/-} C57B6/J mice. Cisplatin was intraperitoneally injected to the tumor-bearing mice, and the mice were sacrificed on the 18th day after the commencement of cisplatin treatment (figure 4D). In wild-type mice, knockout of miR-21 in MTCQ1 cells potentiated the tumor suppressive effect of cisplatin, whereas the miR-21 knockout-potentiated chemotherapy response was

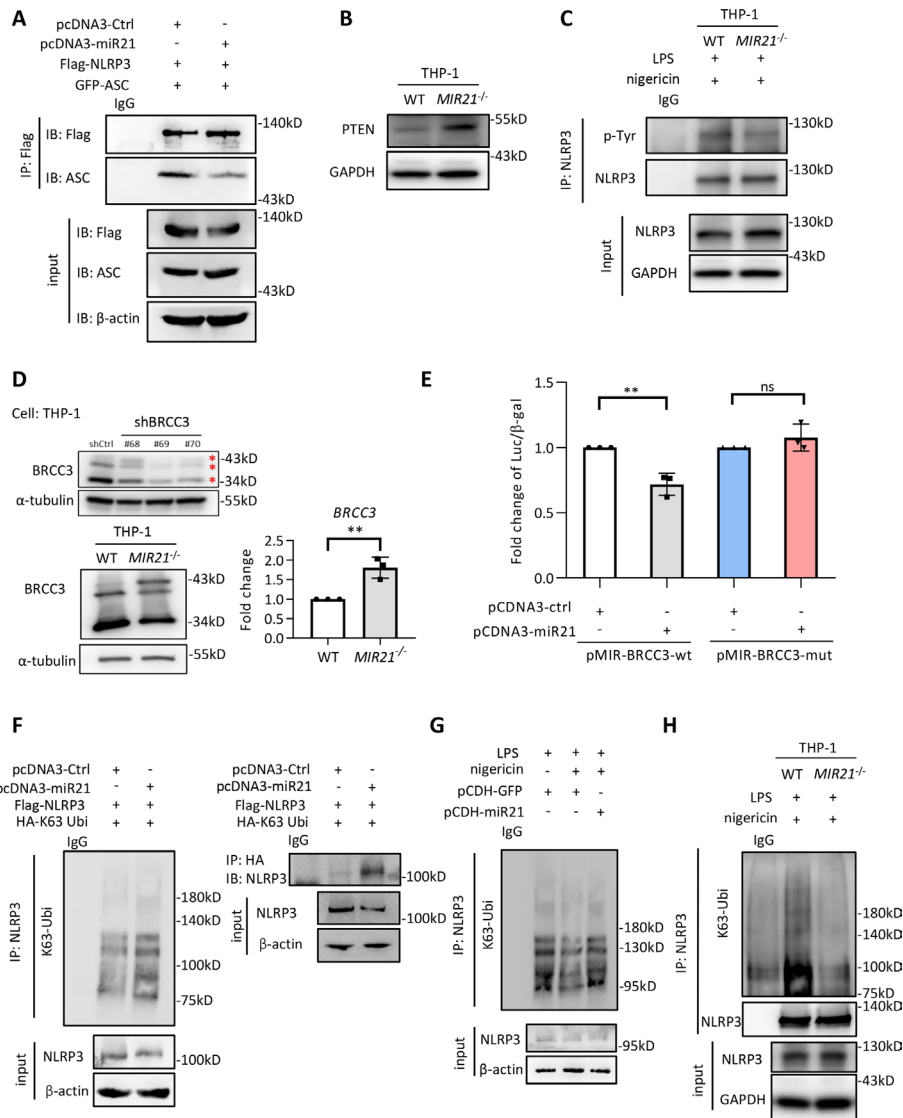


Figure 3 The miR-21-containing exosomes represses *BRCC* and *PTEN* to reduce NLRP3 inflammasome activity. (A) Immunoprecipitation (IP)-western blots to show the interaction of NLRP3 and ASC in HEK293T cells transfected with Flag-NLRP3, GFP-ASC and miR-21/control vector. IgG is a control for IP. (B) Immunoblots for examining the expression of PTEN in macrophages derived from THP-WT or THP1^{MIR21-/-}. (C) IP-western blots to show the tyrosine phosphorylation of THP-WT/THP1^{MIR21-/-}-derived macrophages primed by LPS (1 μ g/mL) and activated by nigericin (5 μ M). IgG is a control for IP. (D) Left upper, western blot of BRCC3 in THP1 cells receiving short hairpin RNA against BRCC3. Left lower, western blots of BRCC3 in THP-WT/THP1^{MIR21-/-}-derived macrophages. α -tubulin was a loading control. Right, quantitative real-time PCR for examining the relative expression of *BRCC3* in THP-WT/THP1^{MIR21-/-}-derived macrophages. n=3 (each contains two technical replicates). Data shows mean \pm SD. **p<0.01 by Student's t-test. (E) *BRCC3* 3'-UTR reporter assay. The wild-type or miR-21 binding site mutated 3'-UTR reporter constructs of *BRCC3* (pMIR-BRCC3-wt and pMIR-BRCC3-mut), pcDNA3-miR21/control vector and β -galactosidase were co-transfected to HEK293T cells. Data represent means \pm SD. **p<0.01 by Student's t-test. n=3 independent experiments (each contains two technical replicates). (F) IP-western blot to show the K63-ubiquitylated NLRP3 in HEK293T cells transfected with miR-21 or a control vector. NLRP3 (left panel) or HA-tagged K63 ubiquitin (right panel) was immunoprecipitated for immunoblotting. IgG is a control for IP. (G) IP-western blot to show the K63-ubiquitylated NLRP3 in THP1-derived activated macrophages primed by LPS (1 μ g/mL) and transfected with miR-21 or a control vector. Nigericin (5 μ M) was used to activate inflammasome. IgG is a control for IP. (H) IP-western blot to show the K63-ubiquitylated NLRP3 in THP1-WT/THP1^{MIR21-/-}-derived activated macrophages. IgG is a control for IP. miR, micro RNA; UTR, untranslated region.

abrogated in *Nlrp3*^{-/-} mice (figure 4E-F). We examined whether cisplatin influence the viability of TAMs from murine MTCQ-WT and MTCQ^{mir21-/-}-formed tumors by 7-Aminoactinomycin D (7-AAD). The result showed that cisplatin treatment had a slight trend to reduce the viability of F4/80⁺ macrophages in MTCQ-WT-formed

tumors, and the effect was also noted in MTCQ^{mir21-/-}-formed tumors (online supplemental figure 6B). We next investigated the impact of inflammasome activation on pyroptosis of human THP1 cells-derived macrophages. Knockout of miR-21 increased LPS/nigericin-induced cleavage of gasdermin D and IL-1 β . A SYTOX green assay

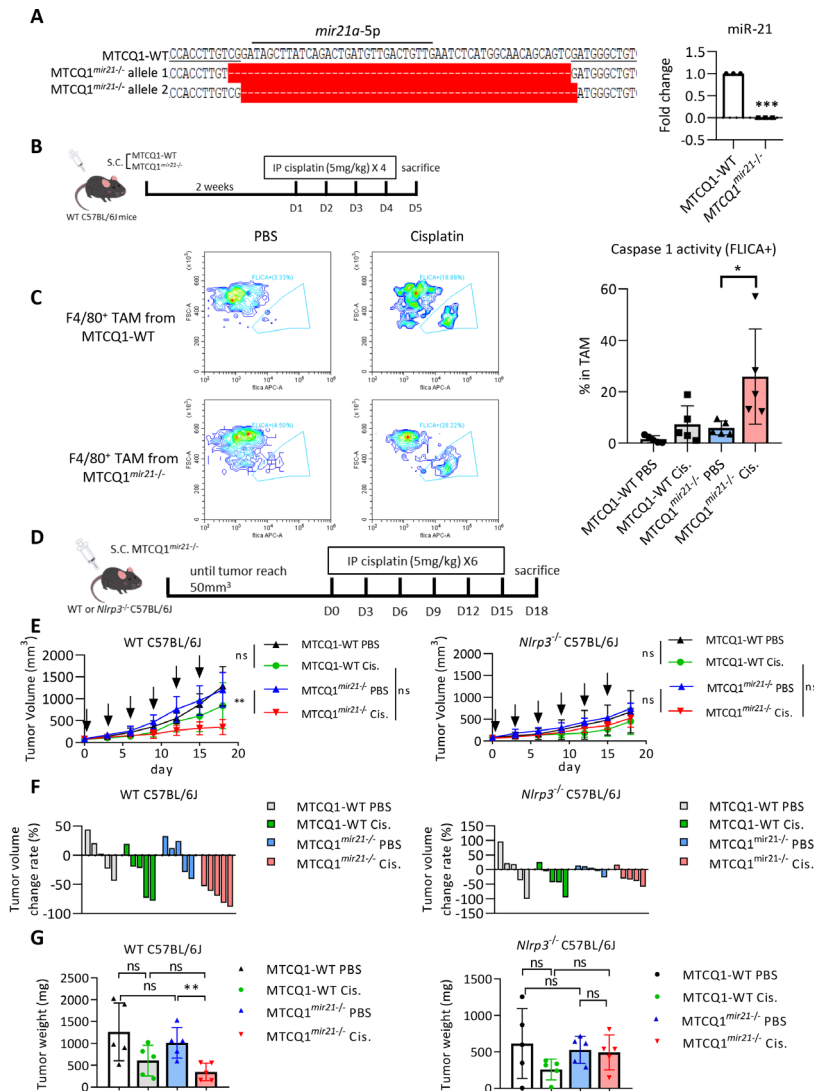


Figure 4 Depletion of mir-21 potentiates response to chemotherapy in oral cancer cells. (A) Left, genomic sequence of mir21a-5p of wild-type murine oral cancer cell line MTCQ1 (MTCQ-WT) and mir-21 knockout subline MTCQ1^{mir21-/-}. Right, quantitative real-time PCR for analyzing the expression of mir-21 of MTCQ-WT and MTCQ1^{mir21-/-}. Data represent means±SD. ***p<0.001 by Student's t-test. n=3 independent experiments (each experiment contains two technical replicates). (B) Schema of the experiment for assaying inflammasome activities of murine tumors. 1×10⁶ of MTCQ1-WT or MTCQ1^{mir21-/-} cells were inoculated to the subcutaneous region of the wild-type C57BL/6J mice for 2 weeks. Cisplatin 5 mg/kg was given intraperitoneally for 4 consecutive days. The mice were sacrificed on the fifth day after the start of cisplatin injection. F4/80⁺ tumor associated macrophages (TAMs) were harvested and caspase 1 activity (FLICA⁺) was analyzed by flow cytometry. (C) Left, representative data of the flow cytometry analysis for the caspase 1 activity of the TAMs (F4/80⁺FLICA⁺) after treated with cisplatin or the control PBS. n=5 for each group. Data shows mean±SD. *p<0.05 by Student's t-test. (D) Schema of the experiment of (E) and (F). 1×10⁶ of wild-type MTCQ1 cells (MTCQ1-WT) or MTCQ1^{mir21-/-} cells were inoculated to the subcutaneous region of the wild-type or Nlrp3^{-/-} C57BL/6J mice. After the tumor size reached 50 mm³ (day 0), intraperitoneal injection of cisplatin (50 mg/kg) or PBS was given every 3 days for a total of six doses, and the tumor size were measured every 3 days. Mice were sacrificed at the 18th day and tumor weight were measured. (E) The volume the MTCQ1-WT/MTCQ1^{mir21-/-}-formed tumors in wild-type or Nlrp3^{-/-} mice treated with cisplatin or PBS. n=5 for each group. Data shows mean±SD. **p<0.01, ns=no significance by Student's t-test. (F) The waterfall plots to indicate the tumor volume change of each mouse. (G) The weight of the MTCQ1-WT/MTCQ1^{mir21-/-}-formed tumors in wild-type or Nlrp3^{-/-} mice treated with cisplatin or PBS. n=5 for each group. Data shows mean±SD. **p<0.01 ns=no significance by Student's t-test. miR, micro RNA; PBS, phosphate buffered saline.

also validated the increased pyroptosis in macrophages derived from THP1^{MIR21-/-} cells. Re-expression of miR-21 in THP1^{MIR21-/-} cells reduced SYTOX green-stained cells (online supplemental figure 6C-D).

We next investigated the effect of Snail on chemotherapy-induced inflammasome activation in vivo.

The murine mammary cancer cell line 4T1 transfected with Snail or a control vector (4T1-Snail/4T1-control; online supplemental figure 7A) was intravenously injected into BALB/c mice to establish pulmonary colonization of tumors. Cisplatin was administered 14 days after the tumor cell injection. Mice were euthanized 3

days later, and the F4/80⁺ macrophages were isolated from the lungs of mice to investigate NLRP3 inflammasome activation by PLA (figure 5A). Overexpression of Snail in murine 4T1 cells significantly reduced the interaction between NLRP3 and ASC in F4/80⁺ macrophages (figure 5B). A reduced level of serum IL-1 β was noted in mice that received orthotopic implantation of 4T1-Snail and were subsequently treated with cisplatin compared with the 4T1-control group (online supplemental figure 7B). We used another syngeneic mouse model to confirm the effect of Snail on the suppression of inflammasome activation. We delivered shRNA against Snail or a control sequence into the murine Lewis lung carcinoma cell line LLC1 (LLC1-shSnail or LLC1-control, respectively; online supplemental figure 7C). LLC1-shSnail/LLC1-control cells were inoculated into the subcutaneous area of wild-type or *Nlrp3*^{-/-} C57BL/6J mice. Cisplatin was injected 10 days after tumor cell inoculation, and the mice were euthanized on the 13th day (figure 5C). In wild-type mice, knockdown of Snail in cancer cells increased the interaction between NLRP3 and ASC in TAMs and the serum level of IL-1 β . NLRP3-ASC interaction in TAMs was not observed in *Nlrp3*^{-/-} mice, as expected (figure 5D). The elevation of serum IL-1 β in the LLC1-shSnail group was also not noted in *Nlrp3*^{-/-} mice (figure 5E).

We next confirmed the role of the Snail-regulated NLRP3 inflammasome in chemotherapy responses. The effect of Snail knockdown exerted on chemotherapy-mediated tumor suppression, the recruitment of interferon (IFN)- γ -expressing CD8⁺ tumor-infiltrating lymphocytes (TILs), and the expression of *Ifng* were examined in the LLC1 syngeneic mouse model (the gating strategy of CD45⁺CD8⁺IFN- γ ⁺ TILs is illustrated in online supplemental figure 7D). When mice were not treated with cisplatin, knockdown of Snail caused a borderline decrease in tumor volume/weight. In contrast, the effect of Snail-knockdown-induced tumor suppression was augmented when mice received cisplatin treatment (figure 5F–G). IL-1 β affects CD8⁺ T cells to enhance their effector function in response to antigen stimulation.^{14 41} The present study found that the knockdown of Snail increased the proportion of IFN- γ -expressing CD8⁺ TILs after cisplatin treatment (figure 5H). Suppression of Snail also enhanced the expression of *Ifng* in the harvested tumors (figure 5I). To further validate the Snail-miR-21 axis in regulating tumor response to cisplatin, we generated the murine LLC1-sh-ctrl, LLC1-sh-Snail, and LLC1-sh-Snail-miR21 sublines for in vivo experiments. The expression of Snail and miR-21 was validated in the corresponding cell lines (online supplemental figure 7E). Snail knockdown potentiated the effect of cisplatin treatment, and the expression of miR-21 in Snail-knockdown LLC1 cells abrogated this effect (online supplemental figure 7F–G). Taken together, these results suggest that Snail attenuates cisplatin-induced NLRP3 inflammasome activation of TAMs, which contributes to the chemoresistance of cancer cells.

Tumorous miR-21 repopulates the infiltrated immune cells in syngeneic tumors

To understand the influence of miR-21 expression in chemotherapy-treated oral cancers on infiltrated immune cells, scRNA-seq was performed using the CD45⁺ cells sorted from the wild-type/miR21 knockout murine oral cancer MTCQ1 cell (MTCQ-WT/MTCQ^{mir21-/-})-derived tumors 72 hours after chemotherapy (online supplemental figure 8A; online supplemental table 8). We used CIPR to annotate the cell clusters of the CD45⁺ cells,²¹ and different types of immune cells were identified accordingly (figure 6A and online supplemental figure 8B). The following pattern of infiltrated immune cells was distinct between the wild-type and miR-21 KO cancer cell-derived tumors: a significant increase in the proportion of macrophages, dendritic cells, monocytes, and natural killer cells and a decrease in the proportion of CD4⁺ T cells and regulatory T cells were noted in murine MTCQ^{mir21-/-}-derived tumors (figure 6B).

Next, we analyzed the TAMs in MTCQ-WT- and MTCQ^{mir21-/-}-derived tumors. The results showed that TAMs from MTCQ^{mir21-/-}-derived tumors harbored an immunoactive gene signature compared with that from MTCQ-WT-derived tumors (figure 6C, online supplemental table 9). GO analysis revealed that the pathways related to immune responses and inflammation were significantly enriched in TAMs of MTCQ1^{mir21-/-}-derived tumors (figure 6D, online supplemental table 10). GSEA demonstrated that compared with the TAMs of MTCQ1-WT-derived tumors, TAMs of MTCQ^{mir21-/-}-derived tumors were associated with a more significant reactive oxygen species-related signature and downregulated expression of the TGF- β -related signature (figure 6E). Since the polarity of macrophages affects the therapeutic efficacy of tumors significantly,⁴² we further analyzed the subclusters of TAMs in these two groups (figure 6F; online supplemental table 11). Re-clustering of macrophages demonstrated a distinct distribution of macrophage subgroups among TAMs from MTCQ^{mir21-/-}- and MTCQ-WT-derived tumors. A significantly higher proportion of cluster 1 was noted in the MTCQ1^{mir21-/-} group, whereas a dominant cluster 2 was observed in the MTCQ1-WT group (figure 6G). Pathway analysis showed that TAMs other than cluster 2 TAMs were associated with an immunoactive signature (online supplemental figure 8C), (online supplemental table 12). However, there is no significant trend of M1/M2 polarity among these seven clusters. Cluster 1 macrophages tended to coexpress both M1 and M2 genes compared with the other clusters (online supplemental figure 8D). Single-cell trajectory analysis of the macrophages/monocytes from tumors revealed that the order of macrophage polarization was cluster 6 to clusters 2 and 3, followed by separation into clusters 1, 4, and 5 (online supplemental figure 9A). In addition to the expression signature in macrophages, the gene expression signature was also distinct between the dendritic cells obtained from the MTCQ1^{mir21-/-} and MTCQ1-WT groups

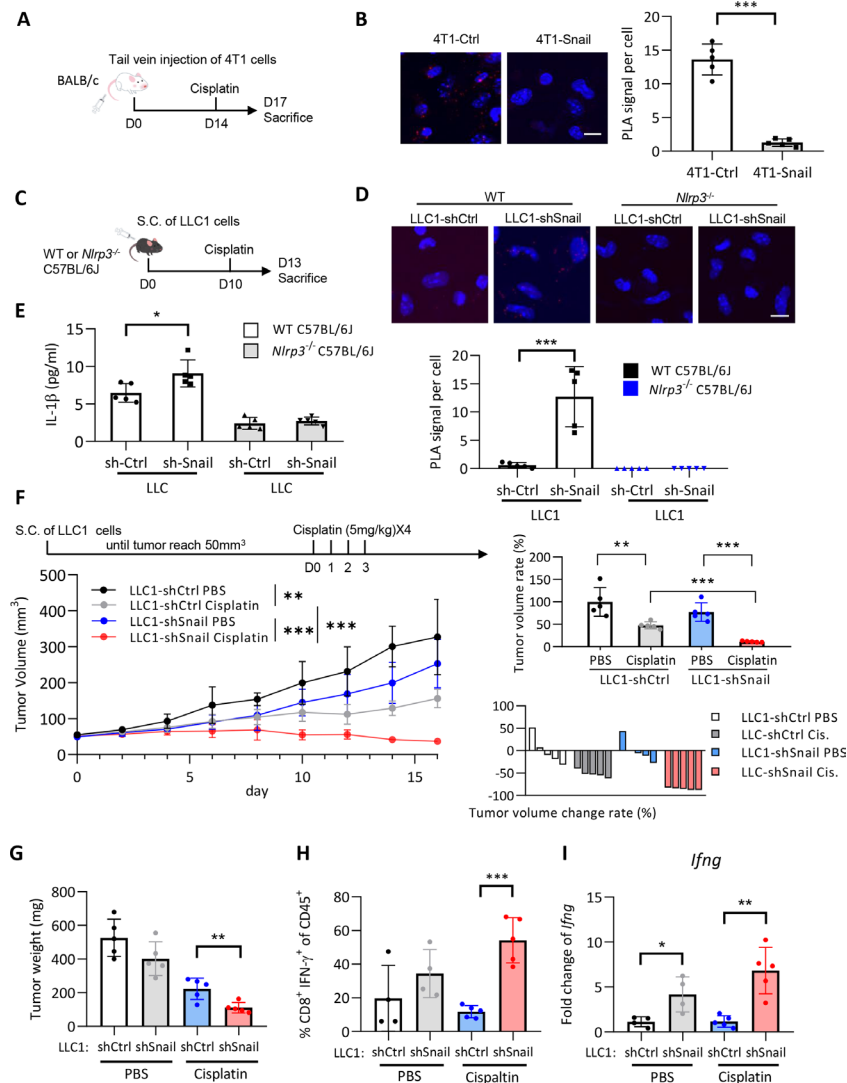


Figure 5 Snail limits chemotherapy-induced NLRP3 inflammasome activation in vivo. (A) Schema of the experiment. 2.5×10^5 4T1 cells expressing Snail or a control vector were intravenously injected into the tail veins of BALB/c mice. 4T1 tumor-bearing mice received a single injection of cisplatin (5 mg/kg) at the 14th day after tumor cell injection. The mice were sacrificed at the 17th day and the F4/80⁺ macrophages isolated from the lungs of the mice were subjected to PLA analysis. (B) PLA signal of NLRP3 and ASC interaction in pulmonary macrophages of 4T1-Snail/4T1-Ctrl. Left, the representative immunofluorescent images for showing the interaction of ASC-NLRP3 in F4/80⁺ macrophages isolated from lungs of mice. The red dots indicate the PLA signals. Right, quantification of PLA signals per cell. For each mouse, four high power fields from random selection were used for PLA quantification. Scale bar, 10 μ m. n=5 for each group. ***p<0.001 by Student's t-test. (C) Schema for animal experiment. 5×10^5 LLC1 cells were inoculated into the subcutaneous area of the WT or *Nlrp3*^{-/-} C57BL/6J mice. A single dose of cisplatin (5 mg/kg) was given at the 10th day after tumor cell injection. The mice were sacrificed at the 13th day after tumor injection. The F4/80⁺ TAMs were harvested for PLA for detecting the NLRP3-ASC interaction. (D) PLA signal of NLRP3 and ASC interaction. Upper, the representative immunofluorescent images for showing the NLRP3-ASC interaction in F4/80⁺ TAMs isolated from tumors. For each mouse, at least a total of 30 cells from eight randomly-selected fields were used for PLA quantification. Lower, quantification of PLA signals per cell. Scale bar, 10 μ m. ***p<0.001 by Student's t-test. (E) Serum IL-1 β level of mice 3 days after cisplatin treatment (n=5). Data shows mean \pm SD. *p<0.05 by Student's t-test. (F) Left upper, schema of the experiment. LLC1 cells (2.5×10^5) were inoculated to the subcutaneous region of C57BL/6 mice. Cisplatin (5 mg/kg) was given at 0, 1, 2, 3 day after tumor cell injection. The mice were sacrificed at the 16th day after cisplatin/PBS treatment. Left lower, tumor volume curve. Right upper, tumor volume change presented in %. Right lower: a waterfall plot to show the volume change of each tumor. n=5 for each group. Tumor volume is shown in mean \pm SD, and tumor volume reduction rate shows mean \pm SD. **p<0.01, ***p<0.001 by Student's t-test. (G) The tumor weight of LLC1-formed tumors in (F). Data shows mean \pm SD. **p<0.01 by Student's t-test. (H) Quantification of the percentages of CD8⁺IFN- γ ⁺ tumor-infiltrating lymphocytes among CD45⁺ tumor-infiltrating leukocytes in different groups of mice as panel (F). The harvested tumors were dissociated and the tumor-infiltrating leukocytes were analyzed by flow cytometry. For PBS groups, n=4; for cisplatin groups, n=5. ***p<0.001 by Student's t-test. (I) Quantitative real-time PCR for analyzing the expression level of *Ifng* in different groups of LLC1-formed tumors as panel (F) and (G). For PBS groups, n=4; for cisplatin groups, n=5. *p<0.05, **p<0.01 by Student's t-test. IFN, interferon; IL, interleukin; PBS, phosphate buffered saline; PLA, proximity ligation assay; TAM, tumor-associated macrophages.

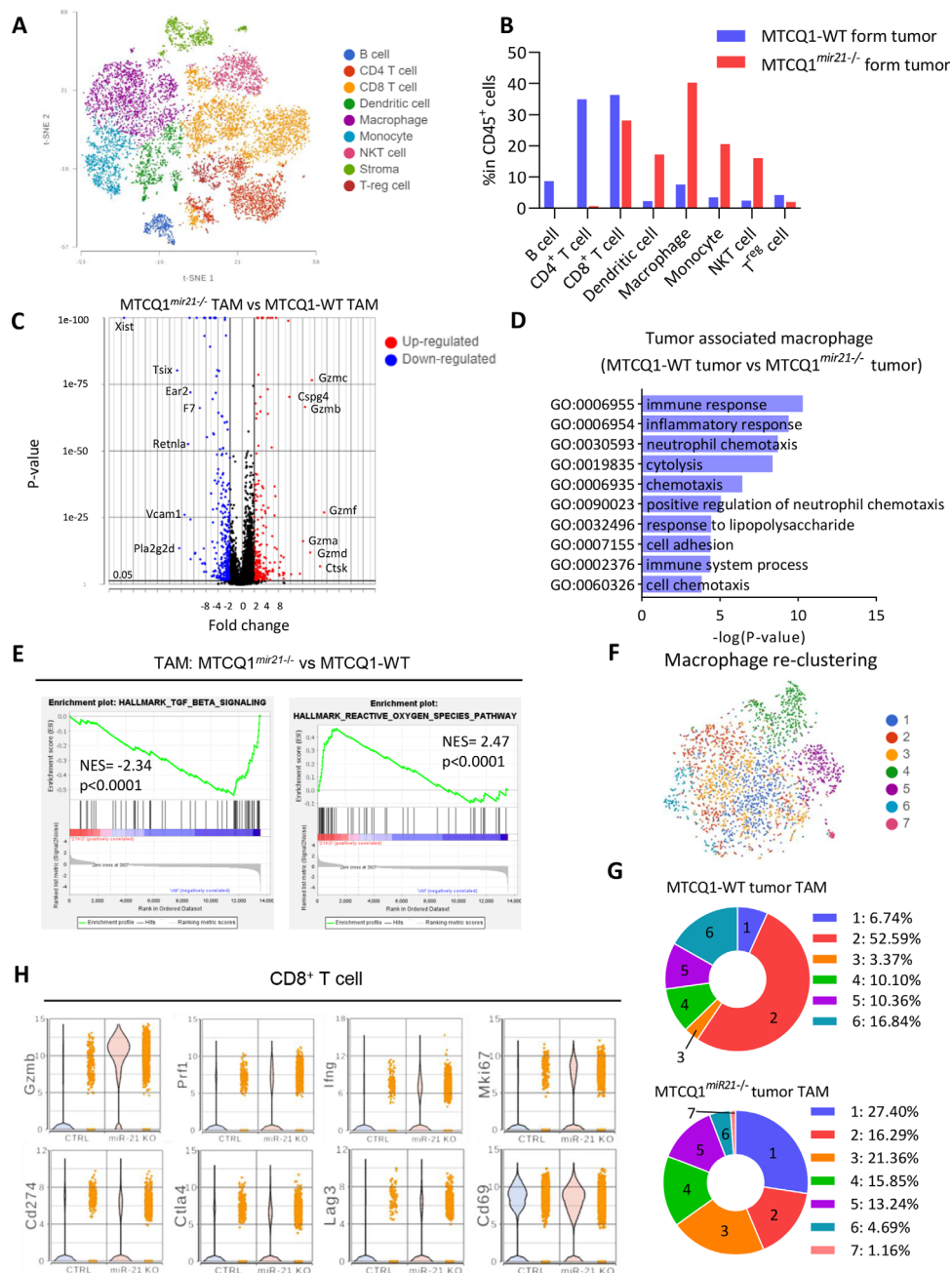


Figure 6 Tumorous mir-21 shapes the infiltrated immune cells of syngeneic murine oral cancers. (A) The t-distributed stochastic neighbor embedding and immune cell type clustering (see Liu *et al*²⁸ of CD45⁺ cells in MTCQ1-WT and MTCQ1^{mir21-/-}-formed tumors 3 days after cisplatin (5 mg/kg) injection. (B) Different immune cell type distribution between MTCQ1-WT and MTCQ1^{mir21-/-}-formed tumor. (C) Volcano plots of the differential expressed genes of the TAMs from MTCQ1^{mir21-/-} versus MTCQ1-WT-formed tumors. Red, upregulated genes; blue, downregulated genes. (D) GO enrichment analysis of the biological pathways of the TAMs from MTCQ1^{mir21-/-} versus MTCQ1-WT-formed tumors. (E) GSEA of the TGF- β signaling gene set (M5896) and reactive oxygen species pathway gene set (M5938) in MTCQ1^{mir21-/-} TAMs versus MTCQ1-WT TAMs. (F) Re-clustering of the TAMs from MTCQ1-WT and MTCQ1^{mir21-/-}-formed tumors. (G) Distribution of the TAM clusters of MTCQ1-WT or MTCQ1^{mir21-/-} TAM. (H) Violin plots for showing the expression of the T cell activation genes (*Gzmb*, *Pf11*, *Ifng*, *Mki67*) and immune checkpoint genes (*Cd274*, *Ctla4*, *Lag3*, *Cd69*) expression in CD8⁺ T cells of the MTCQ1-WT and MTCQ1^{mir21-/-} tumors. GSEA, Gene Set Enrichment Analysis; GO, Gene Ontology; miR, micro RNA; TAM, tumor-associated macrophages; TGF- β : transforming growth factor β .

(online supplemental figure 9B), (online supplemental table 13).

Next, we investigated the influence of tumorous mir-21 expression on the infiltrated T cells. The violin plots showed that knockout of mir-21 in tumor cells increased

the expression of the cytotoxic genes (*Grmb*, *Pf11*), activated T-cell genes (*Ifng*, *Mki67*) in T cells, suggesting that the activity and cytotoxicity of T cell was enhanced in mir-21 knockout tumors. A mild increase of the immune checkpoints (*Cd274*, *Ctla4*, *Lag3*, and *Cd69*) was noted in

TILs of mir-21 knockout tumors (figure 6H). Regarding the expression of the genes related to T cell exhaustion, a reduced *Tcf1* and an increased *Tbet* was noted. The level of *Tim3* and *Pd1* was not changed significantly (online supplemental figure 9C). In summary, these data suggest that an increased antitumor activity of both macrophages and CD8⁺ T cells was observed in the infiltrated immune cells of mir21^{-/-} tumors after chemotherapy.

The Snail-miR-21 axis correlates with the suppression of NLRP3 inflammasome activity and a worse response to chemotherapy in patients with head and neck cancer

Finally, we validated the clinical significance of the Snail-miR-21 axis in the regulation of inflammasome activity and chemosensitivity in patients with HNSCC. We first examine the prognostic impact of Snail, miR-21, and BRCC3 in the HNSCC TCGA database. The result showed that in the total population of TCGA-HNSCC, a higher expression of *SNAIL* was correlated with a worse overall survival ($p=0.03858$). The expression of *BRCC3* and *MIR21* did not have significant impact on the overall survival of HNSCC. We further analyzed the subgroup of patients with HNSCC receiving pharmaceutical treatment ($n=53$). *SNAIL* or *MIR21* upregulation correlated with worse an overall survival, whereas *BRCC3* expression did not have a significant prognostic impact (figure 7A). This result indicates that the Snail-miR-21 axis has a negative impact on patient with HNSCC survival especially in patients receiving pharmaceutical therapies, which is consistent with our hypothesis that the Snail-miR-21 axis influences the treatment responses of patients with HNSCC.

We next confirmed the findings in three independent sets of samples which were used in this study. In the first group, we retrospectively analyzed the expression of *SNAIL* and IFN- γ gene expression signatures in 50 HNSCC samples. Increased expression of *SNAIL* correlated with higher miR-21 and downregulated expression of IFN- γ signature genes *IFN- γ* , *CXCL9*, and *CXCL10* (figure 7B). In the second group, we prospectively collected serum samples from 19 patients with HNSCC who received chemotherapy. The samples were obtained 1 day before and 1 day after chemotherapy to examine the level of IL-1 β to indicate the activity of inflammasomes. The expression of Snail in the corresponding tumors was also examined. In patients with low Snail expression, upregulated serum IL-1 β levels were observed after chemotherapy. When tumors expressed a higher level of Snail (Snail + ~ ++), chemotherapy could not induce a post-treatment surge in IL-1 β levels (figure 7C). The treatment response was concordant with the expression of Snail, that is, a low percentage of tumor response to chemotherapy was noted in patients with Snail +++ (figure 7D). In the third group, we examined the correlation between Snail and activated NLRP3 inflammasome in TAMs in five tumor samples. PLA could detect activation of the NLRP3 inflammasome in tumor samples probed with anti-NLRP3 and anti-ASC antibodies. Immunofluorescence staining

of CD68 was performed to indicate the activation of the NLRP3 inflammasome in TAMs. Reduced abundance of CD68⁺PLA⁺ TAMs was observed in Snail-overexpressing HNSCC cells (figure 7E). In summary, the clinical sample data support that the Snail-miR21 axis regulates the activity of the NLRP3 inflammasome to attenuate the response to chemotherapy in HNSCC.

We summarize our finding in online supplemental figure 10. In cancer cells with high expression of Snail, the tumor-derived exosomes are enriched with miR-21. The miR-21 suppresses the expression of *PTEN* and *BRCC3* in macrophages, which results in the phosphorylation and K63 polyubiquitination of NLRP3, leading to the disassembly and inactivation of NLRP3 inflammasomes. NLRP3 inflammasome inactivation lowers IL-1 β secretion, thereby the chemotherapy-induced inflammation and immunogenic cell death is reduced.

DISCUSSION

Despite the arguments put forth regarding inflammasome activation in cancer progression and therapeutic responses, recent studies support the role of inflammasome activation in augmentation of the chemotherapy response via enhancement of antitumor immunity. Chemotherapy-induced damage-associated molecular patterns include extracellular ATP, a potent activator of the NLRP3 inflammasome,⁴³ which activates the inflammasome of dendritic cells to produce IL-1 β and IL-18 to expand immune signals and to recruit CD8⁺ T-cells for antitumor immune responses.¹⁴ A recent study has shown that phosphorylation of NLRP3 in myeloid cells reduces NLRP3-ASC interaction and inhibits inflammasome activity, resulting in the development of chemoresistance.²⁰ Intriguingly, our clinical data showed that in patients with advanced HNSCC harboring a higher Snail expression, the basal level of serum IL-1 β was relatively high compared with the Snail-low cases. However, the post-treatment surge in IL-1 β levels was not observed in the Snail-high HNSCC and was associated with a worse chemotherapy response (figure 7C–D). The high basal level and lack of response of IL-1 β in Snail-high advanced HNSCC cases implicate pro-tumorous inflammatory microenvironments of aggressive tumors with blunted chemotherapy-triggered inflammasome activation. Together with these findings, our study clarifies the context-dependent role of the inflammasome of innate immune cells in cancer, in which inflammasome-induced proinflammatory signals favor tumor growth. In contrast, therapy-induced inflammasome activation facilitates chemotherapy-induced antitumor immunity and treatment responses.

Our data showed that miR-21 was the most abundant exosomal miRNA in HNSCC, consistent with reports regarding the significant oncogenic role and abundance of miR-21 in different types of cancers.⁴⁴ The miR-21 exerts its oncogenic effects by targeting different tumor suppressors, such as *PTEN*,³⁹ *PDCD4*,⁴⁵ ⁴⁶ and

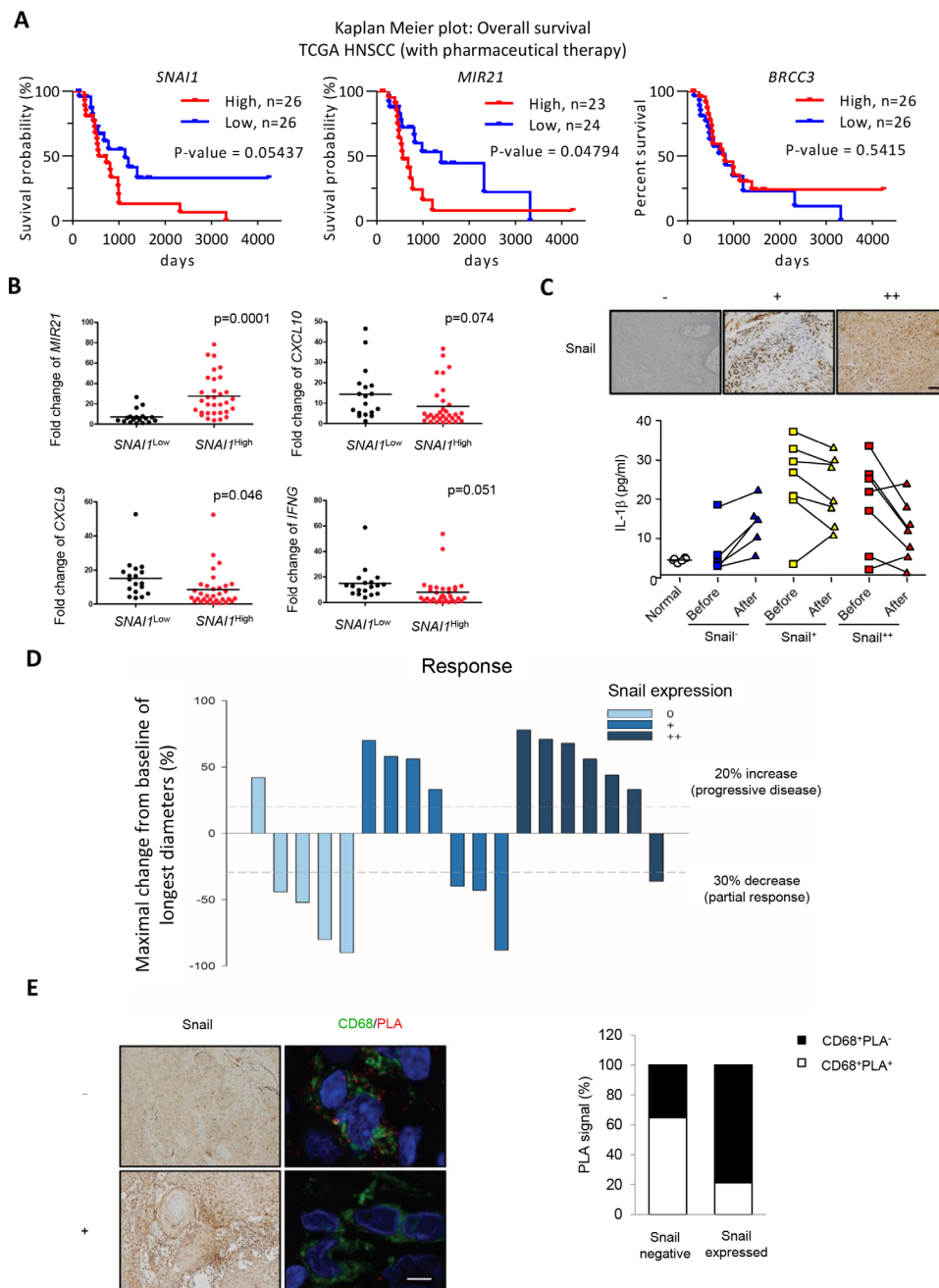


Figure 7 Snail limits chemotherapy-induced NLRP3 inflammasome activation in patients with HNSCC. (A) Kaplan-Meier plots for analyzing the influence of differential expression of *SNAI1*, *MIR21*, and *BRCC3* on overall survival of patients with HNSCC with pharmaceutical therapy from TCGA database. The log-rank p value is shown in each panel. (B) Quantitative real-time PCR for analyzing the expression level of *MIR21*, *CXCL10*, *IFNG* and *SNAI1* in HNSCC samples. n=50. The *SNAI1*^{High} (n=32) is defined as the level higher than mean value, and the *SNAI1*^{Low} (n=18) is defined as the level lower than mean value. (C) Upper, IHC staining of Snail with differential expressions in representative HNSCC samples. Scale bar, 50 μ m. Lower, serum IL-1 β level in patient with HNSCC before and 1 day after chemotherapy. (D) A waterfall plot for illustrating the response to chemotherapy of patients with HNSCC in (C). (E) Left, IHC staining of Snail (left) and immunofluorescent staining (right) of CD68 (green)/NLRP3-ASC PLA (red) in representative HNSCC samples. Right, quantification of the results. Three Snail-negative and two Snail-positive HNSCC samples were used in the experiment. For each sample, at least five CD68⁺ TAMs were quantified for PLA signals. The result is shown as the percentage of PLA-positive among CD68⁺ TAMs. Scale bar, 5 μ m. HNSCC, head and neck squamous cell carcinoma; IHC, immunohistochemistry; PLA, proximity ligation assay; TAM, tumor-associated macrophages; TCGA, The Cancer Genome Atlas.

*IGFBP3*⁴⁷ to promote tumor growth. However, the role of miR-21 in immune cells is more complicated than its prominent pro-tumorous effects in cancer cells. It is

well established that miR-21 is predominantly expressed in M2 macrophages.^{6 48 49} In this study, we showed that miR-21 suppresses NLRP3 inflammasome activation in

TAMs. Nevertheless, miR-21 has been reported to activate NLRP3 inflammasome in septic shock patients by repressing A20 to activate NF- κ B for increasing the transcription of inflammasome components.³⁶ The possible explanation for the differential role of miR-21 in regulating NLRP3 inflammasome in different disease context is as follows. NLRP3 inflammasome activation can be regulated at both the transcription level of the inflammasome components for regulating the amount of inflammasome subunits and post-translational modification of NLRP3 for regulating inflammasome assembly. In patients with cancer, the primary TMEs contain abundant inflammatory cytokines,⁵⁰ and macrophages in primary tumors expressed both the M1 and M2 phenotype.⁵ We consider that the basal level of the components of NLRP3 inflammasome is relatively high in patients with cancer, the assembly of inflammasome is therefore crucial for regulating its activities. In patients with septic shock, activation of inflammasomes is the triggering event for the subsequent immune response, therefore induction of components of the expression of NLRP3 inflammasome is important.

Compared with the prominent oncogenic role in cancer cells, contradictory findings were noted regarding the antitumor immunity of miR-21. Knockout of mir-21 in mice slowed the proliferation of both CD4⁺ and CD8⁺ cells and accelerated the growth of engrafted tumors.⁵¹ However, tumorous miR-21 is inversely associated with the densities of CD3⁺ and CD45RO⁺ cells in colorectal cancers.⁵² Furthermore, miR-21 promotes M2 polarization,⁴⁹ and our previous work has shown that miR-21-containing TEXs are potent regulators of TAMs through the promotion of M2-like activation.⁶ Here, we further investigated the role of Snail-miR-21 axis in antitumor immunity. Snail-driven miR-21-abundant TEXs inhibited NLRP3 inflammasome activity of macrophages. In HNSCC, an increased infiltration of TAMs was observed in samples with a higher expression of Snail (online supplemental figure 1A). Knockout of mir-21 in the murine oral cancer cell line MTCQ (MTCQ^{mir21-/-}) upregulated caspase-1 activity of TAMs when treated with cisplatin (figure 4C). In the scRNA-seq analysis, knockout of mir-21 reduced the proportion of CD4⁺ TILs but activated CD8⁺ TILs. Regarding the innate immune cells, depletion of mir-21 prominently enriched and shaped the gene expression signature of innate immune cells such as macrophages and dendritic cells to an antitumor profile (figure 6). Taken together, we consider that the malignant behaviors of miR-21-abundant cancers are attributed to both the oncogenic effect of intracancerous miR-21 and the TME-modulating effect of exosomal miR-21. In tumor-infiltrated immune cells, miR-21 may majorly affect innate immune cells in response to stimuli, highlighting the importance of exosomal transmission of miR-21.

In conclusion, we demonstrate the development of an immune adaptation-related chemoresistance driven by Snail during metastatic evolution. The plasticity of cancer

cells dynamically shapes the tumor-infiltrated immune cells in response to therapeutic stimuli, indicating the necessity of real-time adjustment of treatment strategies alongside tumor progression.

Acknowledgements We thank Professor Shie-Liang Hsieh (Genomics Research Center of Academia Sinica, Taiwan) and Nien-Jung Chen (Institute of Microbiology and Immunology, National Yang Ming Chiao Tung University, Taiwan) for providing the *Nlrp3*^{-/-} C57BL/6 mice and technique supports; Dr Szu-Ting Chen (Institute of Clinical Medicine, National Yang Ming Chiao Tung University, Taiwan) for the pcDNA3-Flag-NLRP3 plasmids and critical comments; Tri-Biotech (Taiwan) for technical support related to the exosomal micro RNA sequencing; Dr Tsai-Yu Tzeng (Cancer Progression Research Center, National Yang Ming Chiao Tung University, Taiwan) for providing the sgRNA/Cas9 expression vector and assistance in the CRISPR/Cas9 technology; and Man-Ting Yu (National Yang Ming Chiao Tung University University) for the excellent technical support. We thank Division of Experimental Surgery, Department of Surgery of Taipei Veterans General Hospital for the assistance in processing clinical samples.

Contributors M-HY is the guarantor of the study and supervised the whole study. M-HY, H-YC, and C-HH conceived and designed the experiments. H-YC and C-HH performed most of the experiments with the help of P-HL, Y-TC, and DS-SH; and they analyzed the data. M-HY, S-KT and P-YC provided clinical samples and patient care. M-HY collected all demographic data, interpreted the immunohistochemistry results, analyzed the relevant clinical parameters, and performed the statistical comparisons. H-YC, C-HH and M-HY wrote the paper.

Funding This work was supported by grants from the Ministry of Science and Technology (109-2320-B-010-042 and 108-2314-B-010-020-MY3 to M-HY); the National Health Research Institutes (NHRI-EX109-10919B1 to M-HY); Taipei Veterans General Hospital (V110C-139 and V109E-007-01 to M-HY); Featured Areas Research Center Program within the framework of the Higher Education Sprout Project by the Ministry of Education (to M-HY), and the Ministry of Health and Welfare, Center of Excellence for Cancer Research (MOHW110-TDU-B-211-144019 to M-HY).

Competing interests None declared.

Patient consent for publication Not applicable.

Ethics approval This study involves human participants and was approved by Institutional Review Board of Taipei Veterans General Hospital (TVGH-IRB certificate No. 2014-03-004AC; No. 2017-05-013AC; No. 2018-06-001BC). Participants gave informed consent to participate in the study before taking part.

Provenance and peer review Not commissioned; externally peer reviewed.

Data availability statement Data are available upon reasonable request.

Supplemental material This content has been supplied by the author(s). It has not been vetted by BMJ Publishing Group Limited (BMJ) and may not have been peer-reviewed. Any opinions or recommendations discussed are solely those of the author(s) and are not endorsed by BMJ. BMJ disclaims all liability and responsibility arising from any reliance placed on the content. Where the content includes any translated material, BMJ does not warrant the accuracy and reliability of the translations (including but not limited to local regulations, clinical guidelines, terminology, drug names and drug dosages), and is not responsible for any error and/or omissions arising from translation and adaptation or otherwise.

Open access This is an open access article distributed in accordance with the Creative Commons Attribution Non Commercial (CC BY-NC 4.0) license, which permits others to distribute, remix, adapt, build upon this work non-commercially, and license their derivative works on different terms, provided the original work is properly cited, appropriate credit is given, any changes made indicated, and the use is non-commercial. See <http://creativecommons.org/licenses/by-nc/4.0/>.

ORCID iDs

Han-Ying Cheng <http://orcid.org/0000-0003-0047-4743>

Po-Han Lin <http://orcid.org/0000-0003-2099-6258>

Muh-Hwa Yang <http://orcid.org/0000-0002-8918-1244>

REFERENCES

- 1 Marine J-C, Dawson S-J, Dawson MA. Non-Genetic mechanisms of therapeutic resistance in cancer. *Nat Rev Cancer* 2020;20:743–56.

- 2 Ye X, Weinberg RA. Epithelial-Mesenchymal plasticity: a central regulator of cancer progression. *Trends Cell Biol* 2015;25:675–86.
- 3 Shibue T, Weinberg RA. EMT, CSCs, and drug resistance: the mechanistic link and clinical implications. *Nat Rev Clin Oncol* 2017;14:611–29.
- 4 Hsu DS-S, Wang H-J, Tai S-K, *et al.* Acetylation of snail modulates the cytokinome of cancer cells to enhance the recruitment of macrophages. *Cancer Cell* 2014;26:534–48.
- 5 Lee C-C, Lin J-C, Hwang W-L, *et al.* Macrophage-Secreted interleukin-35 regulates cancer cell plasticity to facilitate metastatic colonization. *Nat Commun* 2018;9:3763.
- 6 Hsieh C-H, Tai S-K, Yang M-H. Snail-overexpressing cancer cells promote M2-like polarization of tumor-associated macrophages by delivering miR-21-abundant exosomes. *Neoplasia* 2018;20:775–88.
- 7 Dongre A, Weinberg RA. New insights into the mechanisms of epithelial-mesenchymal transition and implications for cancer. *Nat Rev Mol Cell Biol* 2019;20:69–84.
- 8 Kudo-Saito C, Shirako H, Takeuchi T, *et al.* Cancer metastasis is accelerated through immunosuppression during snail-induced EMT of cancer cells. *Cancer Cell* 2009;15:195–206.
- 9 Dongre A, Rashidian M, Reinhardt F, *et al.* Epithelial-To-Mesenchymal transition contributes to immunosuppression in breast carcinomas. *Cancer Res* 2017;77:3982–9.
- 10 Taki M, Abiko K, Ukita M, *et al.* Tumor immune microenvironment during epithelial-mesenchymal transition. *Clin Cancer Res* 2021;27:4669–79.
- 11 Li C-W, Xia W, Huo L, *et al.* Epithelial-Mesenchymal transition induced by TNF- α requires NF- κ B-mediated transcriptional upregulation of Twist1. *Cancer Res* 2012;72:1290–300.
- 12 Katsura A, Tamura Y, Hokari S, *et al.* ZEB1-regulated inflammatory phenotype in breast cancer cells. *Mol Oncol* 2017;11:1241–62.
- 13 Guo H, Callaway JB, Ting JP-Y. Inflammasomes: mechanism of action, role in disease, and therapeutics. *Nat Med* 2015;21:677–87.
- 14 Ghiringhelli F, Apetoh L, Tesniere A, *et al.* Activation of the NLRP3 inflammasome in dendritic cells induces IL-1 β -dependent adaptive immunity against tumors. *Nat Med* 2009;15:1170–8.
- 15 Allen IC, TeKippe EM, Woodford R-MT, *et al.* The NLRP3 inflammasome functions as a negative regulator of tumorigenesis during colitis-associated cancer. *J Exp Med* 2010;207:1045–56.
- 16 Huber S, Gagliani N, Zenewicz LA, *et al.* IL-22BP is regulated by the inflammasome and modulates tumorigenesis in the intestine. *Nature* 2012;491:259–63.
- 17 Ershaid N, Sharon Y, Doron H, *et al.* Nlrp3 inflammasome in fibroblasts links tissue damage with inflammation in breast cancer progression and metastasis. *Nat Commun* 2019;10:4375.
- 18 Kroemer G, Galluzzi L, Kepp O, *et al.* Immunogenic cell death in cancer therapy. *Annu Rev Immunol* 2013;31:51–72.
- 19 Son S, Shim D-W, Hwang I, *et al.* Chemotherapeutic agent paclitaxel mediates priming of NLRP3 inflammasome activation. *Front Immunol* 2019;10:1108.
- 20 Huang Y, Wang H, Hao Y, *et al.* Myeloid PTEN promotes chemotherapy-induced NLRP3-inflammasome activation and antitumor immunity. *Nat Cell Biol* 2020;22:716–27.
- 21 Ekiz HA, Conley CJ, Stephens WZ, *et al.* CIPR: a web-based R/ shiny APP and R package to annotate cell clusters in single cell RNA sequencing experiments. *BMC Bioinformatics* 2020;21:191.
- 22 Huang DW, Sherman BT, Lempicki RA. Systematic and integrative analysis of large gene Lists using David bioinformatics resources. *Nat Protoc* 2009;4:44–57.
- 23 Subramanian A, Tamayo P, Mootha VK, *et al.* Gene set enrichment analysis: a knowledge-based approach for interpreting genome-wide expression profiles. *Proc Natl Acad Sci U S A* 2005;102:15545–50.
- 24 Yang M-H, Hsu DS-S, Wang H-W, *et al.* Bmi1 is essential in Twist1-induced epithelial-mesenchymal transition. *Nat Cell Biol* 2010;12:982–92.
- 25 Yang W-H, Lan H-Y, Huang C-H, *et al.* Rac1 activation mediates Twist1-induced cancer cell migration. *Nat Cell Biol* 2012;14:366–74.
- 26 Chae YK, Chang S, Ko T, *et al.* Epithelial-Mesenchymal transition (EMT) signature is inversely associated with T-cell infiltration in non-small cell lung cancer (NSCLC). *Sci Rep* 2018;8:2918.
- 27 Yadav A, Kumar B, Datta J, *et al.* Il-6 promotes head and neck tumor metastasis by inducing epithelial-mesenchymal transition via the JAK-STAT3-SNAIL signaling pathway. *Mol Cancer Res* 2011;9:1658–67.
- 28 Liu C-Y, Xu J-Y, Shi X-Y, *et al.* M2-Polarized tumor-associated macrophages promoted epithelial-mesenchymal transition in pancreatic cancer cells, partially through TLR4/IL-10 signaling pathway. *Lab Invest* 2013;93:844–54.
- 29 Hwang W-L, Yang M-H, Tsai M-L, *et al.* Snail regulates interleukin-8 expression, stem cell-like activity, and tumorigenicity of human colorectal carcinoma cells. *Gastroenterology* 2011;141:279–91. 91 e1–5.
- 30 Peinado H, Alečković M, Lavotshkin S, *et al.* Melanoma exosomes educate bone marrow progenitor cells toward a pro-metastatic phenotype through Met. *Nat Med* 2012;18:883–91.
- 31 Zhou W, Fong MY, Min Y, *et al.* Cancer-secreted miR-105 destroys vascular endothelial barriers to promote metastasis. *Cancer Cell* 2014;25:501–15.
- 32 Baltimore D, Boldin MP, O'Connell RM, *et al.* MicroRNAs: new regulators of immune cell development and function. *Nat Immunol* 2008;9:839–45.
- 33 Iorio MV, Croce CM. MicroRNA dysregulation in cancer: diagnostics, monitoring and therapeutics. A comprehensive review. *EMBO Mol Med* 2012;4:143–59.
- 34 Hwang W-L, Jiang J-K, Yang S-H, *et al.* MicroRNA-146A directs the symmetric division of Snail-dominant colorectal cancer stem cells. *Nat Cell Biol* 2014;16:268–80.
- 35 Vetter G, Saumet A, Moes M, *et al.* miR-661 expression in SNAI1-induced epithelial to mesenchymal transition contributes to breast cancer cell invasion by targeting nectin-1 and StarD10 messengers. *Oncogene* 2010;29:4436–48.
- 36 Xue Z, Xi Q, Liu H, *et al.* miR-21 promotes NLRP3 inflammasome activation to mediate pyroptosis and endotoxin shock. *Cell Death Dis* 2019;10:461.
- 37 Juliana C, Fernandes-Alnemri T, Kang S, *et al.* Non-Transcriptional priming and deubiquitination regulate NLRP3 inflammasome activation. *J Biol Chem* 2012;287:36617–22.
- 38 Py BF, Kim M-S, Vakifahmetoglu-Norberg H, *et al.* Deubiquitination of NLRP3 by BRCC3 critically regulates inflammasome activity. *Mol Cell* 2013;49:331–8.
- 39 Meng F, Henson R, Wehbe-Janek H, *et al.* MicroRNA-21 regulates expression of the PTEN tumor suppressor gene in human hepatocellular cancer. *Gastroenterology* 2007;133:647–58.
- 40 Chen Y-F, Chang K-W, Yang I-T, *et al.* Establishment of syngeneic murine model for oral cancer therapy. *Oral Oncol* 2019;95:194–201.
- 41 Ben-Sasson SZ, Wang K, Cohen J, *et al.* IL-1 β strikingly enhances antigen-driven CD4 and CD8 T-cell responses. *Cold Spring Harb Symp Quant Biol* 2013;78:117–24.
- 42 DeNardo DG, Ruffell B. Macrophages as regulators of tumour immunity and immunotherapy. *Nat Rev Immunol* 2019;19:369–82.
- 43 Mariathasan S, Weiss DS, Newton K, *et al.* Cryopyrin activates the inflammasome in response to toxins and ATP. *Nature* 2006;440:228–32.
- 44 Bautista-Sánchez D, Arriaga-Canon C, Pedroza-Torres A, *et al.* The promising role of miR-21 as a cancer biomarker and its importance in RNA-based therapeutics. *Mol Ther Nucleic Acids* 2020;20:409–20.
- 45 Frankel LB, Christoffersen NR, Jacobsen A, *et al.* Programmed cell death 4 (PDCD4) is an important functional target of the microRNA miR-21 in breast cancer cells. *J Biol Chem* 2008;283:1026–33.
- 46 Asangani IA, Rasheed SAK, Nikolova DA, *et al.* MicroRNA-21 (miR-21) post-transcriptionally downregulates tumor suppressor PDCD4 and stimulates invasion, intravasation and metastasis in colorectal cancer. *Oncogene* 2008;27:2128–36.
- 47 Yang CH, Yue J, Pfeffer SR, *et al.* MicroRNA-21 promotes glioblastoma tumorigenesis by down-regulating insulin-like growth factor-binding protein-3 (IGFBP3). *J Biol Chem* 2014;289:25079–87.
- 48 Caescu CI, Guo X, Tesfa L, *et al.* Colony stimulating factor-1 receptor signaling networks inhibit mouse macrophage inflammatory responses by induction of microRNA-21. *Blood* 2015;125:e1–13.
- 49 Xue J, Xiao T, Wei S, *et al.* miR-21-regulated M2 polarization of macrophage is involved in arsenicosis-induced hepatic fibrosis through the activation of hepatic stellate cells. *J Cell Physiol* 2021;236:6025–41.
- 50 Greten FR, Grivnickov SI. Inflammation and cancer: triggers, mechanisms, and consequences. *Immunity* 2019;51:27–41.
- 51 He W, Wang C, Mu R, *et al.* Mir-21 is required for anti-tumor immune response in mice: an implication for its bi-directional roles. *Oncogene* 2017;36:4212–23.
- 52 Mima K, Nishihara R, Nowak JA, *et al.* MicroRNA MIR21 and T cells in colorectal cancer. *Cancer Immunol Res* 2016;4:33–40.

Supplementary Materials for

Snail-Regulated Exosomal MicroRNA-21 Suppresses NLRP3 Inflammasome Activity to Enhance Cisplatin Resistance

Han-Ying Cheng, Chia-Hsin Hsieh, Po-Han Lin, Yu-Tung Chen, Dennis Shin-Shian Hsu, Shyh-Kuan Tai, Pen-Yuan Chu, and Muh-Hwa Yang

Supplementary materials include:

Supplementary methods with references

10 supplementary figures with legends

Legends for 14 supplementary tables

Supplementary methods

HNSCC patients

The patient characteristics are presented in the corresponding supplementary tables. The first group comprised nine cases of multiplex immunofluorescence staining (supplementary figure 1A, supplementary table 1). The second group comprised frozen samples of 65 dissected tumors derived from 21 HNSCC patients and contralateral normal oral epithelia (supplementary table 2). Bulk RNA sequencing was performed for tumors and normal samples (figure 1B). The third group included 50 samples and the contralateral normal oral epithelia (supplementary table 3). The relative expression levels of *SNAIL*, miR-21, *CXCL9*, *CXCL10*, and *IFNG* were determined by analyzing the fold changes in the tumor tissues compared with their normal counterparts (figure 7B). The fourth group included 19 HNSCC patients who received chemotherapy at the Taipei Veterans General Hospital. The tumor tissues were subjected to staining with an anti-Snail antibody for the categorization of patients (supplementary table 4). The serum levels of IL-1 β before and after chemotherapy were determined before and 1 d after chemotherapy (figure 7C-D). RECIST criteria was applied to define response to chemotherapy¹. For partial response, at least a 30% decrease in the sum of diameters of target lesions, taking as reference the baseline sum diameter. For progressive disease, at least a 20% increase in the sum of diameters of target lesions, taking as reference the smallest sum on study (this includes the baseline sum if that is the smallest on study). In addition to the relative increase of 20%, the sum must also demonstrate an absolute increase of at least 5 mm. The fifth group comprised six paraffin-embedded samples from HNSCC patients receiving treatment at the Taipei Veterans General Hospital (supplementary table 5). The samples were used for PLA/immunofluorescence staining to determine the NLRP3 inflammasome activity in TAMs (figure 7E).

RNA-seq analysis of HNSCC patient samples

We used the following two datasets of RNA-seq data derived from HNSCC patients for analysis: TCGA HNSCC (n=521, website: <https://www.cancer.gov/tcga>) and Taipei Veterans General Hospital (TVGH) HNSCC

(21 normal oral epithelia, 35 primary tumors, and 9 metastatic tumors from 21 patients; see supplementary table 2 for the patient characteristics). Data on TCGA HNSCC sequences were downloaded by using Xena² and cBioPortal³ and normalized to Z score or $\log_2(\text{RPM}+1)$ or $\log_2(\text{norm_count}+1)$. We applied the EMT score to categorize the patients. Briefly, EMT score is defined as the average of Z-score mesenchymal markers (*VIM*, *FNI*, *CDH2*, *ITBG6*, *FOXC2*, *MMP2*, *MMP3*, *MMP9*, *SOX10*, *SNAIL*, *SNAI2*, *TWIST1*, *GSC*) / average epithelial marker (*CDH1*, *DSP*, *TJPI*)⁴. We selected and categorized the top one-third EMT score patients as the EMT^{high} subgroup (n=172 for TCGA and n=22 for TVGH) and the lowest one-third EMT score patients as the EMT^{low} subgroup (n=172 for TCGA and n=22 for TVGH). The expression of the genes of interest was compared in the EMT^{high} versus EMT^{low} subgroups of TCGA and TVGH HNSCC cases.

RNA sequencing for exosomal small RNA

For exosomal small RNA sequencing, exosomes were collected, and total RNA extraction was performed. Small RNA fractions were sequenced using the Illumina Genome Analyzer II (Illumina). ConDeTri was used to trim or remove reads according to the quality score. Qualified reads after filtering low-quality data were analyzed using miRDeep2 to clip the 3' adapter sequence, and reads shorter than 18 nucleotides were discarded before performing the alignment of reads to the human and mouse genomes from UCSC. The expression profiles of miRNAs in FaDu exosomes versus SG exosomes are listed in supplementary table 7.

Preparation of conditional media and macrophages

To produce conditioned media using cancer cells, human HNSCC cell lines FaDu/OECM1 with overexpression or knockdown of Snail were cultured in the RPMI 1640 growth medium supplemented with penicillin/streptomycin and 0.5% FBS for 48 h. The supernatant was centrifuged at $2,000 \times g$ for 5 min, and was subsequently collected and stored at -80°C . To prepare human peripheral blood mononuclear cells (PBMC)-derived macrophages, CD14⁺ monocytes were isolated from the whole blood samples obtained from healthy donors and were cultured in the RPMI 1640 medium containing 10% FBS and 20 ng/ml GM-CSF for 5

days. To generate THP-1-derived macrophages, THP-1 cells were subjected to differentiation overnight with 20 ng/ml phorbol 12-myristate 13-acetate. To induce activation of inflammasomes, the cells were primed with 1 µg/ml LPS for 4 h, following by 5 µM nigericin treatment in conditioned media for 1 h. In some experiments, we used 1 µg/ml LPS for 4 h following by 20 ng/ml IFN-γ in conditioned media for 48 h to stimulate PBMC-derived macrophages (supplementary figure 3A and supplementary figure 5A, 5B, 5E, 5F, 5G).

Purification and characterization of tumor-derived exosomes

Exosome purification was performed as per methods described previously⁵. Briefly, exosomes were purified by differential ultracentrifugation. First, the cells were removed from the conditioned medium via centrifugation at $300 \times g$ for 10 min. To remove large dead cells and substantial cell debris, the supernatants were successively centrifuged at increasing speeds ($2,000 \times g$ for 10 min, $10,000 \times g$ for 30 min, the Beckman SW28 rotor). The supernatant was ultracentrifuged at $100,000 \times g$ for 70 min to pellet the exosomes. Exosomes were subjected to washing steps in PBS and were centrifuged at the same high speed (the Beckman TLA-100.3 rotor). The morphology and size distribution of exosomes were analyzed by performing transmission electron microscopy (JEOL JEM-2000EXII, JEOL USA, Inc., Peabody, MA) and nanoparticle tracking analysis (NanoSight LM10-HS, Malvern Panalytical, Malvern, UK), respectively.

Tissue processing and data generation for Visium spatial gene expression

The sample used for Visium spatial gene expression analysis was obtained from the primary tumor of a 65 year-old male suffered from stage 4 oral squamous cell carcinoma. Tissue sections prepare were follow by Visium Spatial Tissue Optimization User Guide Rev D (10x Genomics, CG000239). In brief, frozen samples were cryosectioned on Visium Tissue Optimization Slides. Histology images were taken using Olympus IX83 (10X PH Objective). Library construction was according to the Visium Spatial Gene Expression User Guide. Libraries were loaded at 250 pM and sequenced on a NovaSeq 6000 System (Illumina) using a NovaSeq S4 Reagent Kit (300 cycles, 20012866, Illumina), at a sequencing depth followed the formula provided by the

manufacturer (10X Genomics): Calculate total sequencing depth \geq coverage area x total spots on the capture area x 50000 read pairs/ spots. (Coverage area: 20.8%, 36.1%, 26.8%, 31.5% / Sequencing depth: 96M, 170M, 126M, 146M read pairs) Data processing of Visium data, raw FASTQ files and images were output with Space Ranger software (Version 1.2.1), hg38 reference genome was used for gene alignment. Analyzing of gene sets (inflammasome related genes and EMT genes) and visualization image were produced by Loupe Browser 5.1.0. Analyzing of gene sets of the inflammasome-related genes⁶ and EMT genes⁴, and visualization image were produced by Loupe Browser 5.1.0.

Generation of the *MIR21/mir21* knockout cell line

To generate *MIR21*-knockout THP1 (THP1^{*MIR21*^{-/-}}) and *mir21*-knockout MTCQ1 (MTCQ1^{*mir21*^{-/-}}) cells, the genomic region flanking *MIR21-5p* / *mir21a-5p* was deleted using the CRISPR/Cas9 system. Briefly, THP-1 or MTCQ1 cells were subjected to transfection with pSpCas9(BB)-2A-Puro (PX459) and pEGFP-N3 pSurrogate reporter, and the in-of-flam dTomato signal was sorted by using FACS Aria (BD). The exact deleted sequence of the *MIR21* / *mir21* genome was cloned using the TA Cloning™ Kit (Thermo) and confirmed by conducting direct sequencing (supplementary figure 4C and figure 4A). The depletion of miR-21/mir-21 in THP-1/MTCQ1 cells was confirmed by performing stem-loop reverse transcription-qPCR.

Quantitative RT-PCR

Quantitative PCR was performed using the StepOnePlus real-time PCR system (Applied Biosystems Inc., Foster City, CA, USA). The primer sequences used for real-time PCR are listed in supplementary table 14.

Immunoblotting and immunoprecipitation

These procedures were performed as per previously described protocols⁴. The results were measured using the GE LAS-4000 biomolecular imager (GE Healthcare Inc., Marlborough, MA). The information on antibodies

used in the experiments is listed in supplementary table 14.

Immunohistochemistry (IHC)

The paraffin-embedded tissue sections were subjected to deparaffinization and retrieval, followed by subsection to washing steps with water and blockade with 3% hydrogen peroxide. The samples were washed first with water and subsequently with PBS, after which they were subjected to blockade and stained with antibodies, and were subsequently subjected to enzymatic avidin-biotin complex (ABC)-diaminobenzidine (DAB) staining (Leica Biosystems, Wetzlar, Germany). Nuclei were subjected to counterstaining with haematoxylin. All comparative images were obtained using an identical microscope and camera settings (Olympus BX51; Olympus Corporation, Tokyo, Japan). For scoring the Snail expression by IHC, ten high-power field images were taken from each sample and interpreted by two independent observers. The mean value of the percentage of nuclear Snail-positive cancer cells was calculated and the Snail IHC score was defined as negative, less than 20% of cancer cells with nucleus staining; +, 20-50% of cancer cells with nucleus staining; and ++, >50% of cancer cells with nucleus staining. The information on the antibodies used in the experiments is listed in supplementary table 14.

Multiplex immunofluorescence staining of HNSCC samples

To perform staining of multiple markers, namely CD4, CD8a, CD163, CD68, CD66b, and PanCK, via multiplex immunofluorescence staining, samples were stained using the Opal 7-Color IHC Kit (Akoya Biosciences) and the corresponding antibodies. After the performance of staining, the Vectra Polaris Automated Quantitative Pathology Imaging System (Akoya Biosciences) was used to scan multispectral data using the Form Tissue Analysis Software (Akoya Biosciences). ImageJ was used to unmix the overlapping signals and to measure the positive signal of each slide. A total of nine patients and ten multispectral images from each patient were involved and analyzed. The information on the antibodies used in the experiments is listed in supplementary table 14.

Proximity ligation assay

The proximity ligation assay (PLA) was performed to investigate the proximity of epitopes recognized by the anti-NLRP3 and anti-ASC antibodies, representing the assembly of NLRP3 inflammasomes in macrophages. Briefly, after incubation with primary antibodies, DuoLink® In Situ PLA probes (Merck KGaA, Burlington, MA) were used and incubation was performed for 1 h at 37°C. Subsequent ligation and detection were performed using the DuoLink® In Situ Detection Reagents Red Kit (Merck KGaA, Burlington, MA, USA). Blockade, antibody hybridization, proximity ligation, and detection were performed according to the manufacturer's recommendations. The fluorescence images were captured using the Olympus Fluoview FV10i Laser confocal microscope (Olympus Corporation, Tokyo, Japan) equipped with a 60x oil objective (Olympus UPLSAPO 60XO, NA 1.35) and analyzed using Olympus FV10-ASW Version 3.0. The PLA signal was quantified by measuring the number of red dots per cell. The total number of quantified cells from randomly selected fields is detailed in the corresponding figure legends.

Luciferase reporter assay

For conducting the *BRCC3* 3'-UTR reporter assay, 50 ng of the wild-type or mutated reporter constructs (+985 to +1784 of the transcription start site TSS), 100 ng of a pCMV-β-gal internal control plasmid, and 3 μg of pCDNA3-miR21 or control vector were co-transfected into HEK-293T cells. Luciferase activity was measured after 48 h of incubation.

SYTOX Green assay

The SYTOX Green staining was applied to assay the pyroptotic cells. THP-1 WT or THP-1^{MIR21^{-/-}} were differentiated with PMA (20 ng/ml) and 5×10^5 cells were seeded onto dishes overnight. NLRP3 inflammasome activation was induced by LPS (1 μg/ml) for 4 hours followed by nigericin (5 μM) for 1 hour, then the cell was incubated with RPMI containing SYTOX green (1 μM, S7020, Thermo Fisher Scientific). Cells were measured

by microplate reader for Ex 488 nm and Em 513 nm.

Animal experiments

C57BL/6J and BALB/c mice (6 to 8 weeks old) were purchased from the National Laboratory Animal Center (Taipei, Taiwan) and were housed in a pathogen-free environment (50% humidity and 22 °C). All animals and experiments were conducted by the Institutional Animal Care and Use Committee of National Yang Ming Chiao Tung University and Taipei Veterans General Hospital with approval IDs (IACUC certificate No. 1090514 of National Yang Ming Chiao Tung University and IACUC certificate No. 2013-169 of Taipei Veterans General Hospital). All mice were acclimated for 3 to 7 days before the experiment. Mice were randomized into different experimental groups. Tumor size was measured and recorded using a digital caliper.

The *in vivo* caspase activity assay (figure 4B,C), tumor measurement (figure 4D-F), and single-cell RNA-sequencing analysis (figure 6, supplementary figure 8, supplementary figure 9) were performed using the MTCQ1-C57BL/6J syngeneic murine oral squamous cell carcinoma model⁷. For the *in vivo* caspase-1 activity assay, 1×10^6 MTCQ1-WT or MTCQ1^{mir21-/-} cells were inoculated into the subcutaneous region of the wild-type C57BL/6 mice for 14 days. The mice received intraperitoneal injection of cisplatin (5 mg/kg/day) or phosphate-buffered saline (PBS) since the 14th day for 4 consecutive days. Mice were sacrificed on the 19th day. The tumor specimens were collected, and the F4/80⁺ TAMs were isolated to determine caspase 1 activity (F4/80⁺ FLICA⁺ cells, ImmunoChemistry Technologies, Davis, CA). To measure the size and weight of the tumors, 1×10^6 MTCQ1-WT or MTCQ1^{mir21-/-} cells were inoculated into the subcutaneous region of wild-type or *Nlrp3*^{-/-} C57BL/6J mice. The developed tumors were measured regularly and allowed to grow until the average volume reached 50 mm³ (volume = width² × length/2). Mice received PBS or 5 mg/kg cisplatin daily every 3 days for a total of six doses. The mice were sacrificed on the 18th day, and the weights of the tumors were recorded. For single-cell RNA-sequencing (scRNA-seq) analysis, 1×10^6 MTCQ1-WT or MTCQ1^{mir21-/-} cells were injected into the subcutaneous region of the wild-type C57BL/6J mice for 14 days (n=3 for each group). Intraperitoneal injection of cisplatin 5 mg/kg was administered on the 14th day, and the tumors were harvested

for scRNA-seq analysis.

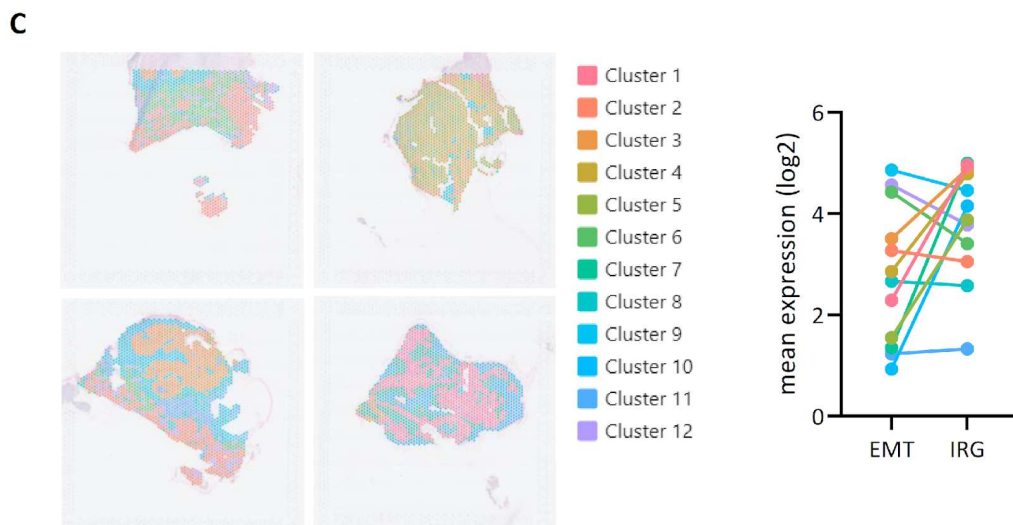
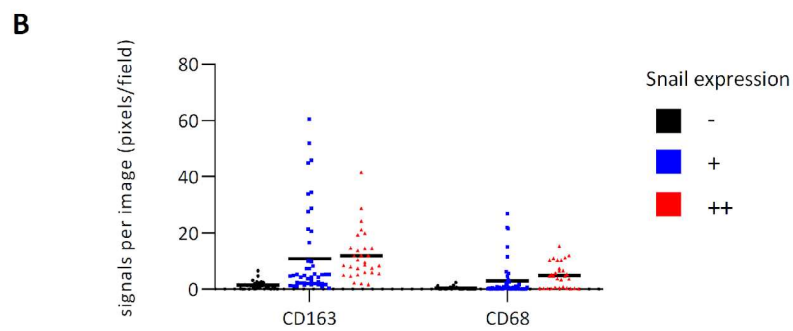
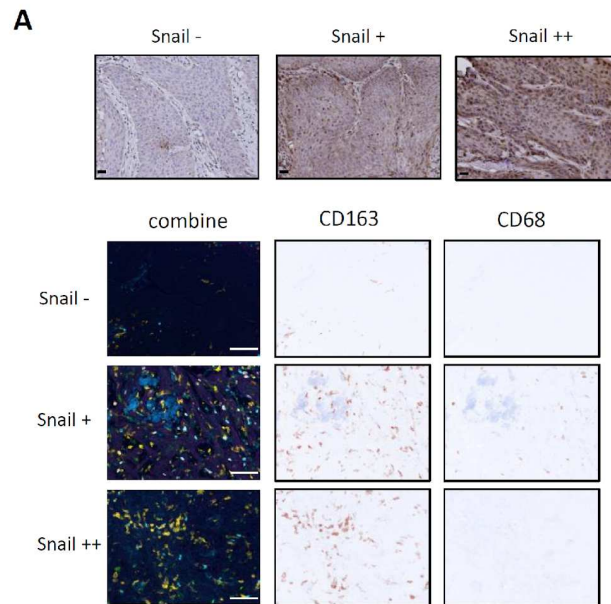
We applied two additional syngeneic murine tumor models, 4T1-BALB/c and LLC-C57BL6/J in the study. *In vivo* PLA and serum IL-1 β levels were detected in both syngeneic models (figure 5A-E, supplementary figure 7). Tumor size and weight were measured, and the infiltrated T cells were analyzed in the LLC-C57BL6/J model (figure 5F-I). For *in vivo* PLA in the 4T1-BALB/c model (figure 5A-B), 2.5×10^5 tumor cells were intravenously injected into the tail veins of the mice. The tumor-bearing mice received a single injection of 5 mg/kg cisplatin on the 14th day after tumor-cell injection. The mice were euthanized on the 17th day after the tumor cell injection. F4/80⁺ macrophages were isolated from the lungs, and PLA was performed using these cells. For measuring serum IL-1 β levels to represent inflammasome activities in the 4T1-BALB/c model (supplementary figure 7B), a total of 5×10^5 4T1 cells expressing Snail or a control vector were injected into the mammary fat pad of BALB/c mice. The tumor-bearing mice received a single intraperitoneal injection of cisplatin (5 mg/kg body weight) on the 10th day after tumor-cell injection. The mice were euthanized on the 13th day after the tumor cell inoculation. The sera were harvested and IL-1 β levels were detected using a mouse IL-1 β ELISA kit. For assaying the viability of tumor-associated macrophages (supplementary figure 7A), 1×10^6 MTCQ1-WT or MTCQ1^{mir21^{-/-}} cells were inoculated into the subcutaneous region of wild-type C57BL/6 mice for 14 days. Mice received intraperitoneal injection of cisplatin (5 mg/kg/day) or PBS since the 14th day for 4 consecutive days. The mice were sacrificed on day 19. The tumor specimens were collected and then stained with 7-aminoactinomycin D (7-AAD) solution (5 μ L in 400 μ L cell sample, Abcam, Cambridge, UK) before analysis. The CD11b⁺F4/80⁺7AAD⁺ TAMs were determined by flow cytometry. For examining PLA and serum IL-1 β levels in the LLC-C57BL/6 model (figure 5C), 5×10^5 LLC1 cells transfected with shRNA against murine Snail or a control sequence were inoculated into the subcutaneous area wild-type or *Nlrp3^{-/-}* C57BL/6J mice. The tumor-bearing mice received a single intraperitoneal injection of 5 mg/kg cisplatin on the 10th day after tumor cell injection. The mice were euthanized on the 13th day after the tumor cell inoculation. The tumors were harvested for PLA and sera were harvested for examining IL-1 β levels. To measure the tumor size in the LLC-C57BL/6 model (figure 5F-G), 5×10^5 LLC cells receiving shRNA against Snail or a control sequence

were injected into the subcutaneous region of the wild-type or *Nlrp3*^{-/-} C57BL/6J mice. The developed tumors were measured regularly and allowed to grow until the average volume reached 50 mm³. Mice received PBS or 5 mg/kg/day for 4 consecutive days for a total of four doses. The mice were sacrificed on the 16th day, and the weights of the tumors were recorded. For quantification of CD8⁺IFN- γ ⁺ T-cell infiltration and *Ifgr* expression in tumors (figure 5H-I), wild-type C57BL/6 mice were inoculated subcutaneously with 2.5×10^5 LLC-Ctrl or LLC-shSnail cells. The developed tumors were measured regularly and allowed to grow until the average volume reached 50 mm³. Mice received PBS or 5 mg/kg cisplatin daily for four consecutive days in the LLC1 model. The mice were euthanized on the 16th day post-cisplatin injection. The tumor-infiltrating CD8⁺ IFN- γ ⁺ T cells were analyzed using flow cytometry. The expression of *Ifgr* in tumors was examined using RT-qPCR (figure 5I).

References

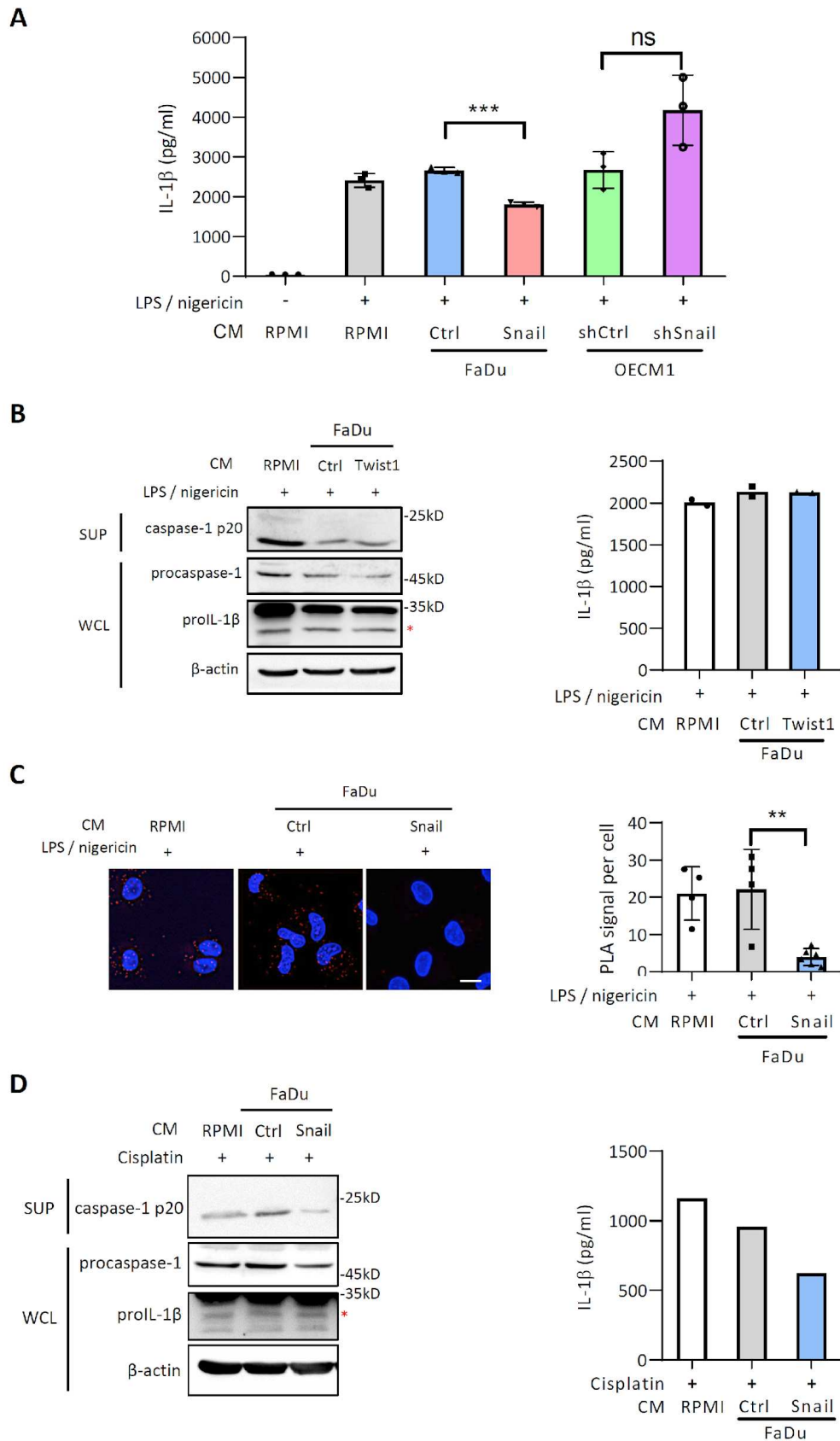
1. Eisenhauer EA, Therasse P, Bogaerts J, Schwartz LH, Sargent D, Ford R, *et al.* New response evaluation criteria in solid tumours: revised RECIST guideline (version 1.1). *Eur J Cancer* **2009**;45:228-47.
2. Goldman MJ, Craft B, Hastie M, Repecka K, McDade F, Kamath A, *et al.* Visualizing and interpreting cancer genomics data via the Xena platform. *Nat Biotechnol* **2020**;38:675-8.
3. Cerami E, Gao J, Dogrusoz U, Gross BE, Sumer SO, Aksoy BA, *et al.* The cBio cancer genomics portal: an open platform for exploring multidimensional cancer genomics data. *Cancer Discov* **2012**;2:401-4.
4. Chae YK, Chang S, Ko T, Anker J, Agte S, Iams W, *et al.* Epithelial-mesenchymal transition (EMT) signature is inversely associated with T-cell infiltration in non-small cell lung cancer (NSCLC). *Sci Rep* **2018**;8:2918.
5. Hsieh CH, Tai SK, Yang MH. Snail-overexpressing cancer cells promote M2-Like polarization of tumor-associated macrophages by delivering miR-21-abundant exosomes. *Neoplasia* **2018**;20:775-88.
6. Zheng T, Wang X, Yue P, Han T,
7. Hu Y, Wang B, *et al.* Prognostic inflammasome-related signature construction in kidney renal clear cell carcinoma based on a pan-cancer landscape. *Evid Based Complement Alternat Med* **2020**;2020:3259795.
8. Chen YF, Chang KW, Yang IT, Tu HF, Lin SC. Establishment of syngeneic murine model for oral cancer therapy. *Oral Oncol* **2019**;95:194-201.

Supplementary Figures



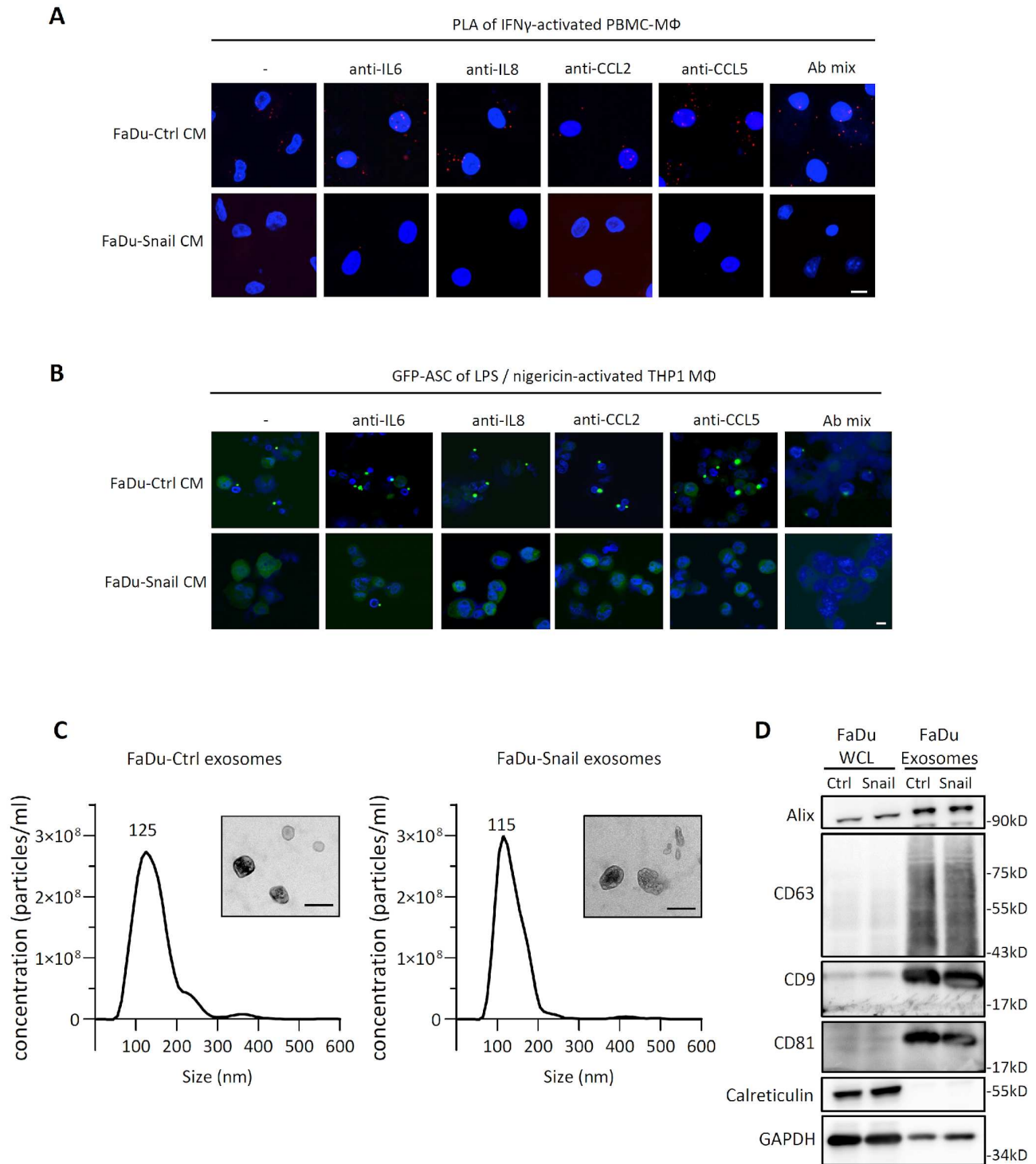
Supplementary figure 1. EMT is associated with the immunosuppressive microenvironments.

- (A) Multiplex immunofluorescent staining in 9 HNSCC samples with differential expression levels of Snail (three cases for each expression level). Upper, representative IHC of Snail. Lower, representative images of multiplex immunofluorescent staining of different markers in Snail (-, +, ++) cases.
- (B) Quantification of the percentage of CD68 and CD163 signals in each image. Each group contains 3 patients and each patient contains 10 randomly selected fields were quantified for the signals. Scale bar=100 μ m.
- (C) Visium spatial transcriptomic analysis of a HNSCC tumor sample. Left, distribution of 12 transcriptomic clusters in the tumor sample. Right, the expression of EMT-related gene and inflammasome-related genes in the 12 clusters. The gene list of the EMT-related genes and inflammasome related genes is shown in supplementary table 3. IRG, inflammasome-related genes.



Supplementary figure 2. The supernatants of Snail-expressing cancer cells inhibit activation of NLRP3 inflammasomes.

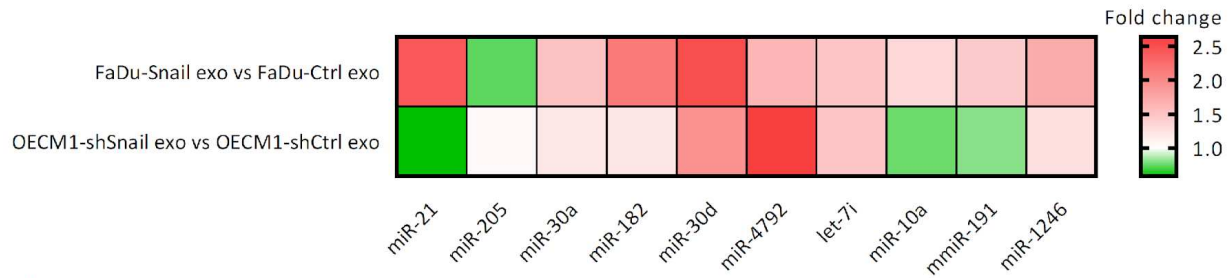
- (A) ELISA for analyzing the level of secreted IL-1 β by LPS/nigericin-activated THP1-derived macrophages incubated with the conditioned media (CM) from FaDu-Ctrl versus FaDu-Snail and OECM1-Ctrl versus OECM1-shSnail. RPMI group was used as a baseline control of ELISA. Data shows mean \pm S.D., n=3 independent experiment (each experiment contains 2 technical replicates). *** $P < 0.001$, ns= no significance by Student's t-test.
- (B) Left, immunoblots of cleaved caspase-1 p20 in supernatants (SUP), pro-caspase-1 and pro-IL-1 β in whole cell lysates (WCL) of LPS/nigericin-activated THP1-derived macrophages incubated with the conditioned media (CM) from FaDu-Ctrl versus FaDu-Twist1 for 24 hr. β -actin was used as a loading control for immunoblots. Right, ELISA for analyzing the level of secreted IL-1 β by activated THP1-derived macrophages in the corresponding groups. Data represent means \pm S.D. n=2 independent experiment (each experiment contains 2 technical replicates).
- (C) Left, proximity ligation assay (PLA) signal of NLRP3 and ASC interaction in LPS/nigericin-stimulated PBMC-derived macrophages incubate with conditioned media from FaDu-Vec or FaDu-Snail. Nigericin was used for inflammasome activation. Scale bar, 10 μ m. Right, quantification of number of PLA signals per cell. For each group, at least a total of fifteen cells from five randomly selected fields (four for FaDu-Ctrl) were used for PLA quantification. Data represent means \pm S.D. ** $P < 0.01$ by Student's t-test.
- (D) Left, immunoblots of cleaved caspase-1 p20 in supernatants (SUP), pro-caspase-1 and pro-IL-1 β in whole cell lysates (WCL) of cisplatin-activated PBMC-derived macrophages incubated with conditioned media from FaDu-Ctrl/FaDu-Snail. β -actin was used as a loading control for immunoblots. Right, ELISA for analyzing the level of secreted IL-1 β by cisplatin-activated macrophages. The data is derived from one independent experiment with 2 technical replicates.



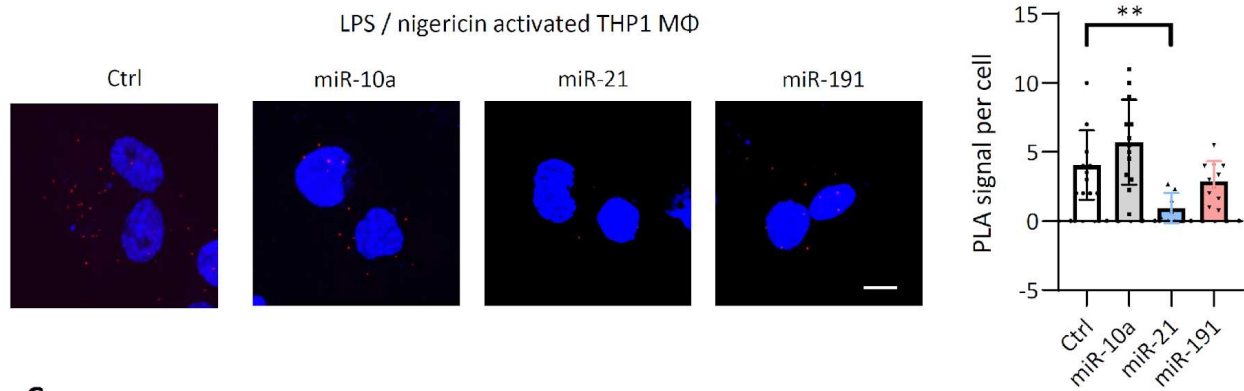
Supplementary figure 3. Snail-expressing cancer cells suppress inflammasome activation and characterization of exosomes secreted by cancer cells.

- (A) PLA for detecting NLRP3 and ASC interaction in IFN- γ -activated PBMC-derived macrophages in conditioned media from FaDu-Ctrl/FaDu-Snail in the presence of neutralizing antibodies as indicated (anti-IL6, antiIL-8, anti-CCL2, anti-CCL5, mix) for 24 h (0.5 μ g/ml). Scale bar, 10 μ m.
- (B) Immunofluorescent images of LPS/nigericin-activated THP1-derived macrophages transfected with GFP-tagged ASC and incubated with conditioned media from FaDu-Ctrl/FaDu-Snail in the presence of indicated neutralizing antibodies (anti-IL6, antiIL-8, anti-CCL2, anti-CCL5, mix) for 24 h. Scale bar, 10 μ m.
- (C) Characterization of exosomes from FaDu-Ctrl/FaDu-Snail by nanoparticle tracking analysis (NTA) and transmission electron microscopy (TEM). The insets show the representative images of TEM. Scale bar=100 nm.
- (D) Western blots for analyzing the expression of Alix, CD63, CD81, CD9, and calreticulin for exosomes and whole cell lysate (WCL) from FaDu-Ctrl/ FaDu-Snail. GAPDH was a loading control.

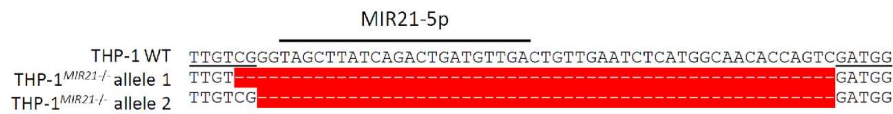
A



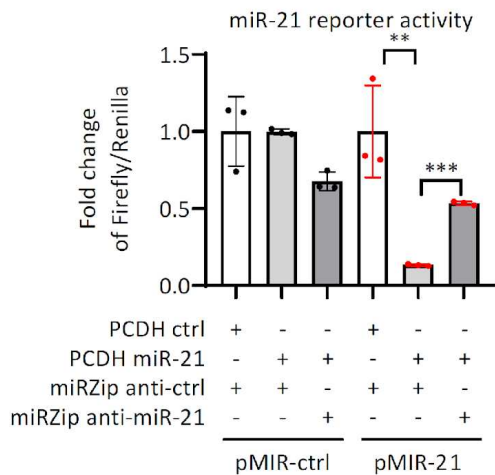
B



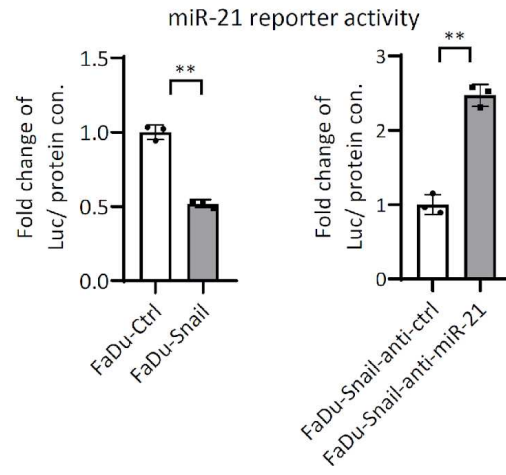
C



D

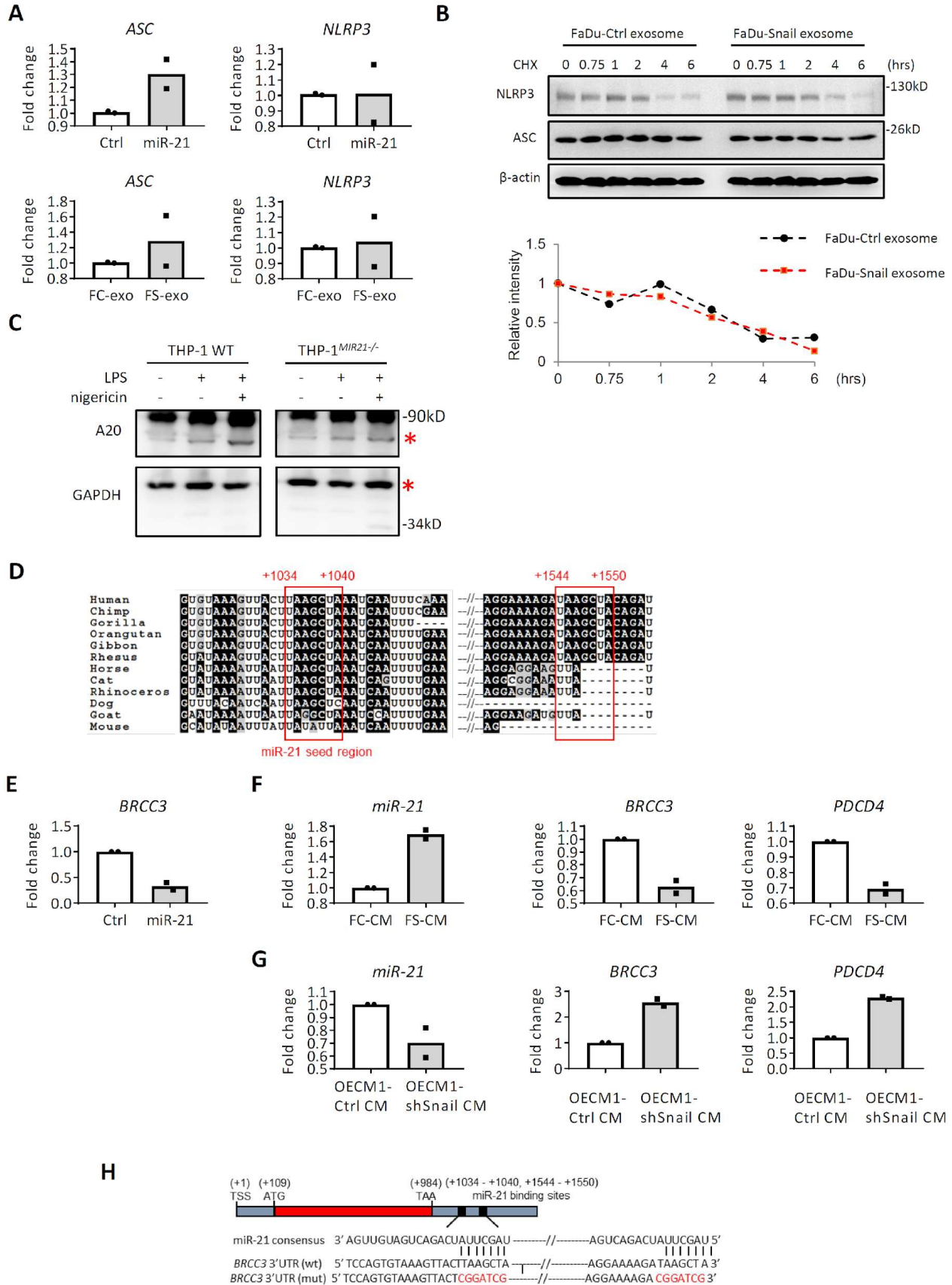


E



Supplementary figure 4. Snail-expressing cancer cells secrete miR-21-abundant exosomes and miR-21 suppress NLRP3 inflammasome activities.

- (A) RT-qPCR for analyzing the exosomal miRNAs derived from FaDu-Ctrl/FaDu-Snail and OECM1-Ctrl/OECM1-shSnail. The selected miRNAs were ranked top 10 in oral cancer-derived exosomes (from exosomal RNA-seq, see Supplementary Table S6). Red, upregulation; green, downregulation. The data is derived from one independent experiment with 2 technical replicates.
- (B) Left, representative images of PLA for detecting NLRP3 and ASC interaction in LPS/nigericin-activated THP-1- derived macrophages transfected with miR-10a, miR-21, miR191, or a control agomir. Scale bar, 10 μm . Right, quantification of number of PLA signals per cell. For each group, at least a total of nineteen cells from randomly selected fields were used for PLA quantification. Data represent means \pm S.D. $**P < 0.01$ by Student's *t*-test.
- (C) Left, genomic sequence of *MIR-21* region of the wild-type THP-1 cell line (THP1-WT) or receiving CRISPR/Cas9 to knock out *MIR21* (THP1^{MIR21^{-/-}}). Right, RT-qPCR for detecting the expression level of expression in THP1-WT and THP1^{MIR21^{-/-}}. n=3 independent experiments (each contains 2 technical replicates). Data shows mean \pm S.D. $**P < 0.01$ by Student's *t*-test.
- (D) A reporter assay for confirming the activity of miRZip anti-miR-21. HEK-293T cells were transfected with the indicated plasmids and the fold change of firefly/renilla luciferase ratio was calculated to represent the relative reporter activity of each condition. Data represent means \pm S.D. n=3 independent experiment (each experiment contains 2 technical replicates). $**P < 0.01$, $***P < 0.001$ by Student's *t*-test.
- (E) A reporter assay for confirming the activity of anti-miR-21 in FaDu-ctrl/FaDu-Snail (left) and FaDu-Snail transfected with anti-miR-21/control sequence (right). Data represent means \pm S.D. n=3 independent experiment (each experiment contains 2 technical replicates). $**P < 0.01$ by Student's *t*-test.

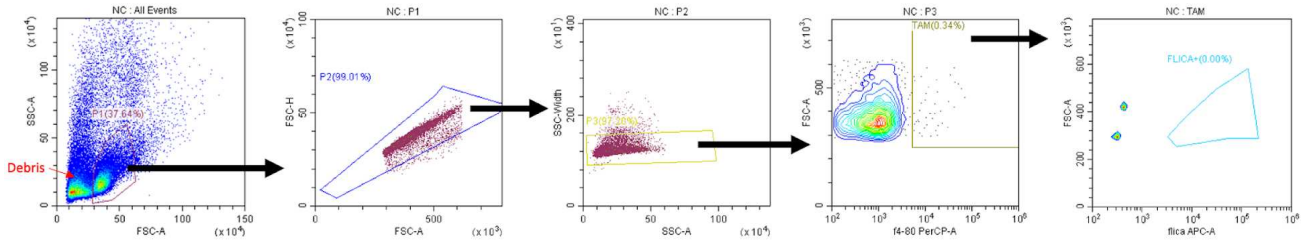


Supplementary figure 5. miR-21 targets the 3'-UTR region of *BRCC3* to suppress its expression.

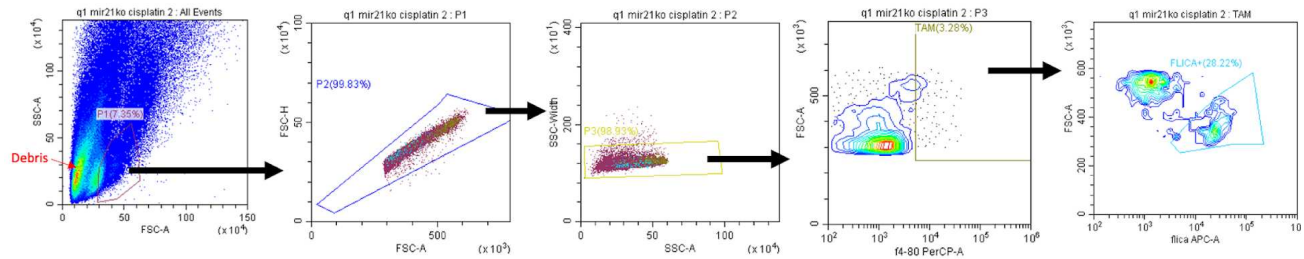
- (A) RT-qPCR for analyzing the expression of ASC and NLRP3 in IFN γ -activated PBMC-derived macrophages transfected with miR-21 or control agomir (upper panels), or macrophages incubated with exosomes from FaDu-Ctrl or FaDu-Snail (FC-exo/FS-exo; upper panels). n=2 independent experiments (each experiment contains 2 technical replicates).
- (B) Upper, western blot of NLRP3 and ASC in IFN γ -activated PBMC-derived macrophages incubated with exosomes derived from FaDu-Ctrl or FaDu-Snail in the presence of cycloheximide (CHX) to inhibit de novo protein synthesis. Lower, relative intensity of NLRP3 protein expression.
- (C) Western blot of A20 in macrophages derived from wild-type THP1 (THP1-WT) or miR-21 knockout THP1 (THP1^{MIR21^{-/-}}). LPS and nigericin were applied for inflammasome activation. GAPDH was a loading control.
- (D) Alignment of the sequences of miR-21 seed regions in *BRCC3* 3'-UTR among different species.
- (E) RT-qPCR of *BRCC3* in IFN γ -activated PBMC-derived macrophages transfected with miR-21 or control agomir. Data represent means \pm S.D. n=2 independent experiments (each experiment contains 2 technical replicates).
- (F) RT-qPCR of miR-21, *BRCC3*, and *PDCD4* in IFN γ -activated PBMC-derived macrophages incubated with conditioned media (CM) from FaDu-Ctrl(FC)/FaDu-Snail(FS) for 48 h. n=2 independent experiments (each experiment contains 2 technical replicates).
- (G) RT-qPCR of miR-21, *BRCC3*, and *PDCD4* in IFN γ -activated PBMC-derived macrophages incubated with conditioned media (CM) from OEMC1-Ctrl/OEMC1-shSnail for 48 h. n=2 independent experiments (each experiment contains 2 technical replicates).
- (H) Representation of the organization of *BRCC3* transcript, and the wild-type or miR-21 binding site mutated 3'-UTR reporter constructs of *BRCC3* (pMIR-*BRCC3*-wt and pMIR-*BRCC3*-mut).

A

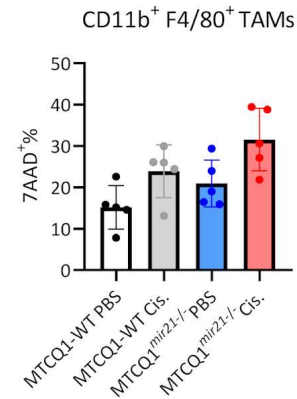
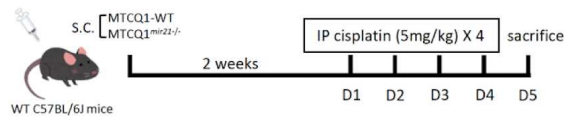
Negative control (no stain)



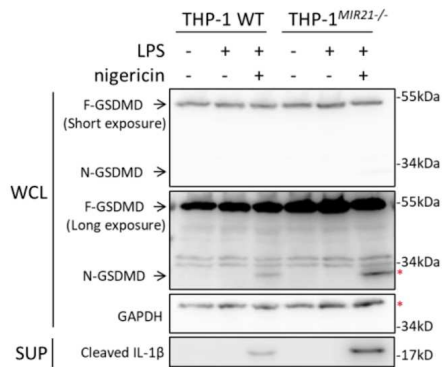
Staining sample



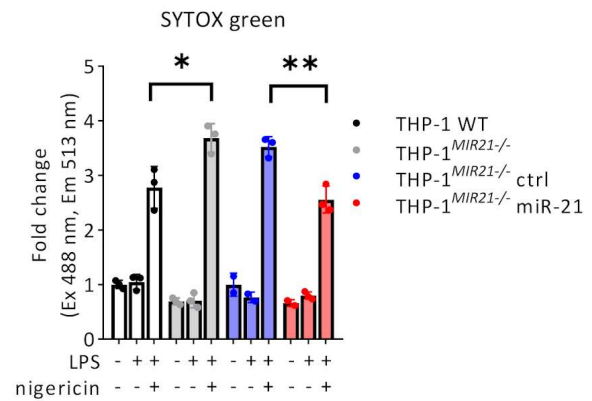
B



C

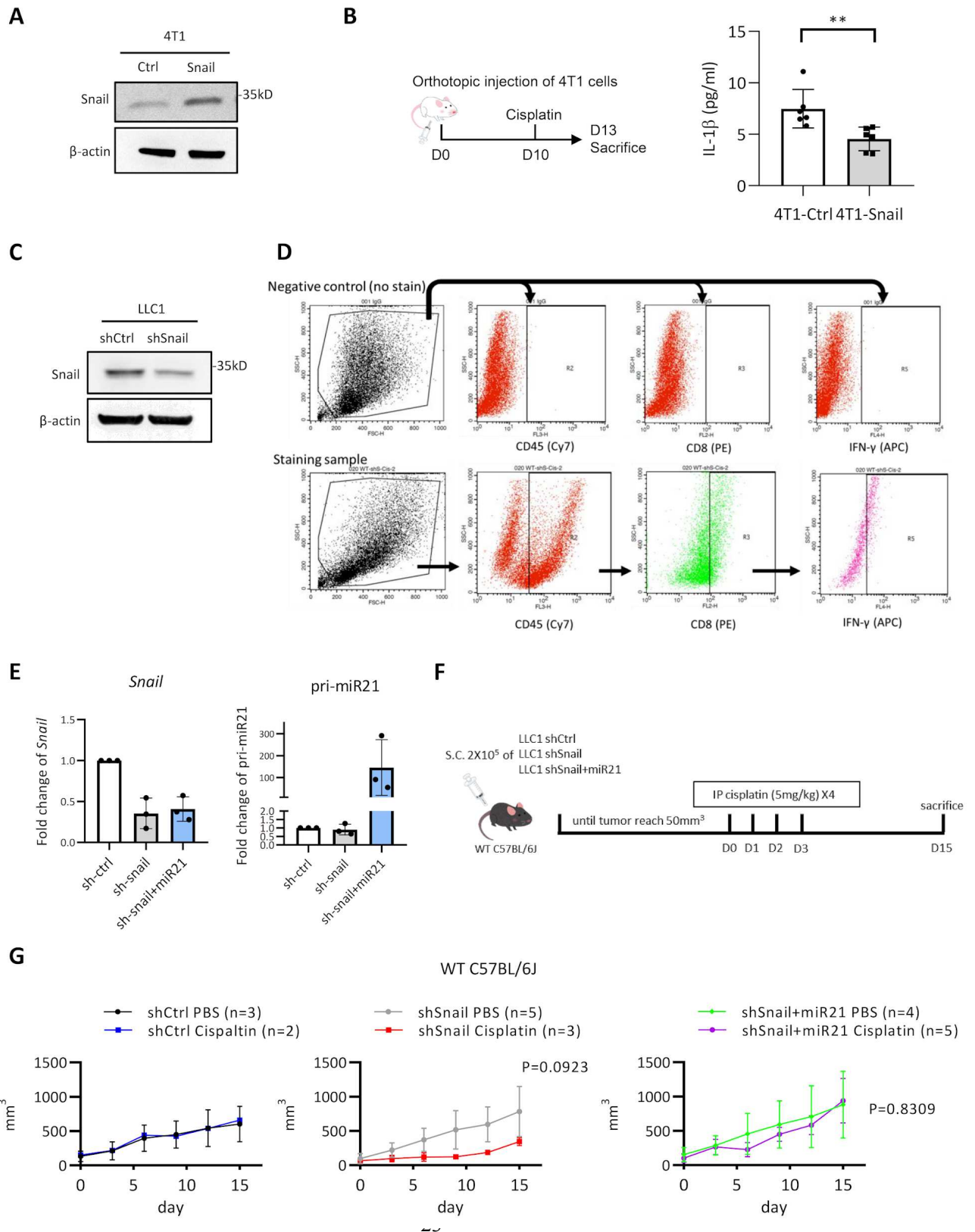


D



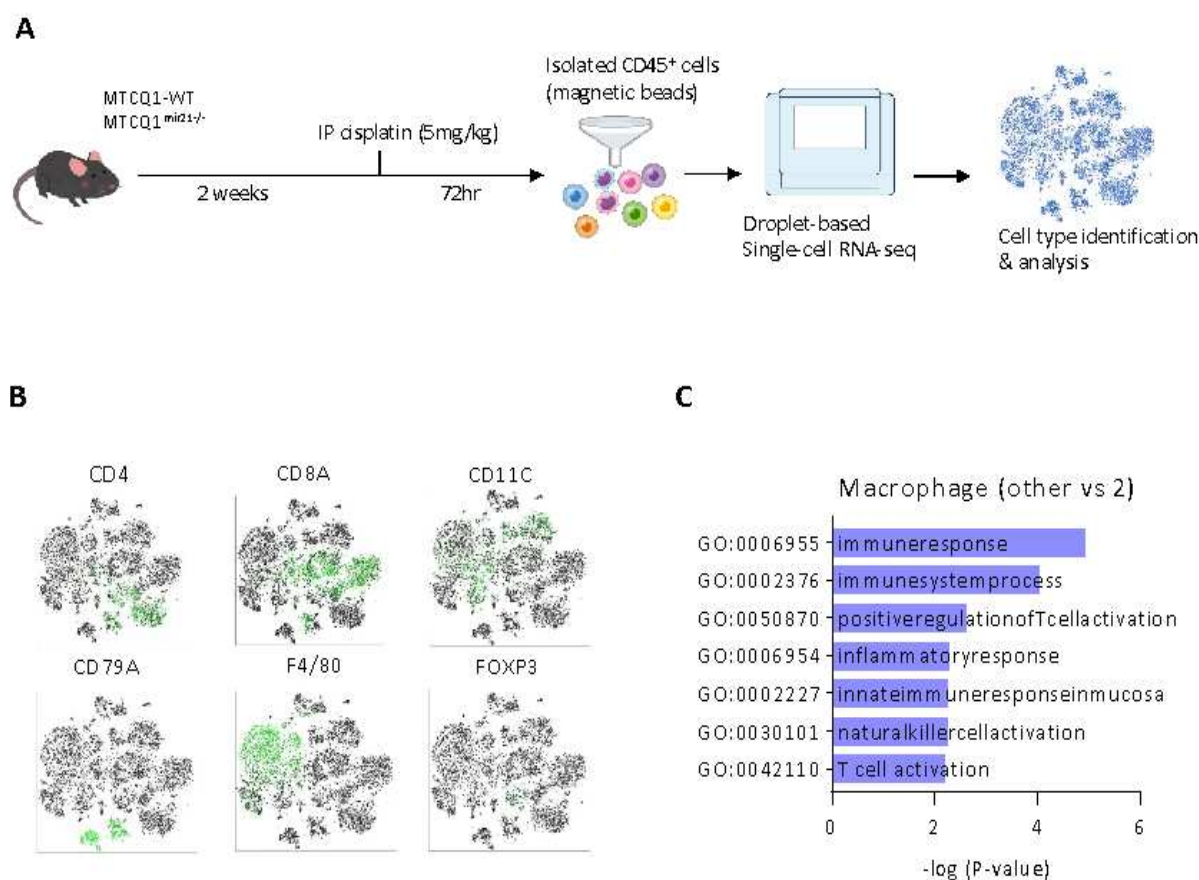
Supplementary figure 6. The influence of miR-21 on the viability and pyroptosis of macrophages.

- (A) Representing results to show the gating strategy of caspase 1-activated F4/80⁺ tumor-associated macrophages detected by FLICA staining in the experiment of figure 4C.
- (B) 7-aminoactinomycin D (7-AAD) staining for examination of the viability of tumor-associated macrophages (TAMs) from murine MTCQ1-WT/MTCQ1^{mir21^{-/-}} cells-formed tumors. CD11b⁺F4/80⁺ TAMs were sorted from the tumors for subsequent analysis. Left, schema of the animal experiment. Right, the percentage of 7-AAD⁺ TAMs from MTCQ1-WT/MTCQ1^{mir21^{-/-}} -formed tumors with or without cisplatin treatment. n=5 for each group. No statistical significance was reached in each comparison.
- (C) Western blots of full length gasdermin D (F-GSDMD), N-terminal gasdermin D (N-GSDMD) of whole cell lysates (WCL) and cleaved IL-1 β of supernatant (SUP) from wild-type THP1 (THP1-WT) or miR-21 knockout THP1 (THP1^{MIR21^{-/-}}) cells with or without LPS/nigericin treatment for inflammasome activation. GAPDH was a loading control.
- (D) SYTOX green assay. THP1-WT/THP1^{MIR21^{-/-}} cells transfected with miR-21 or a control sequence were examined by SYTOX green staining. Inflammasome activation was induced by LPS and nigericin treatment. Cells were measured by microplate reader for Ex 488 nm and Em 513 nm. Data represent means \pm S.D. n=3 independent experiment (each experiment contains 2 technical replicates). * P <0.05, ** P <0.01 by Student's t -test.



Supplementary figure 7. The influence of Snail-mir21 axis on tumor-infiltrated immune cells and tumor growth.

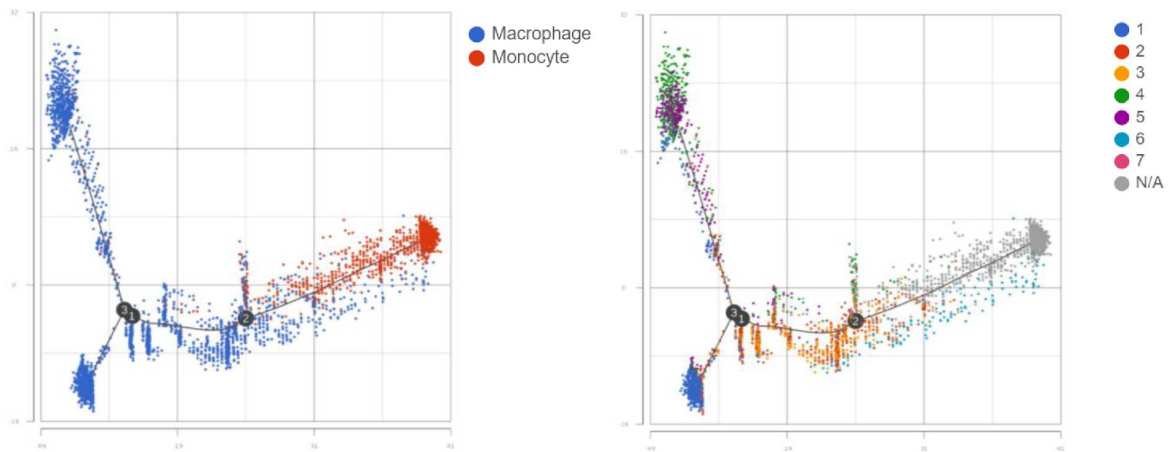
- (A) Western blot of Snail in 4T1 cells transfected with Snail or a control vector (Ctrl). β -actin was a loading control.
- (B) Left, schema of the experiment. Orthotopic implantation of 5×10^5 of 4T1-Ctrl or 4T1-Snail cells into the mammary fat pad of the BALB/c mice. Cisplatin (5 mg/kg) was given at 10th day after tumor cells inoculation. The mice were sacrificed at 13th day for analysis. Right, serum IL-1 β level of mice at 13th day (n= 6). Data represent means \pm S.D. * $P < 0.01$ by Student's *t*-test.
- (C) Western blot of Snail in LLC1 cells receiving an shRNA against Snail (shSnail) or a control sequence (shCtrl). β -actin was used as a loading control.
- (D) Representing results to show the gating strategy of CD45⁺CD8⁺IFN γ ⁺ T cells in the experiment of figure 5H.
- (E) RT-qPCR for examination of the expression of Snail and pri-miR21 in LLC cells expressed a shRNA against Snail (sh-Snail) or a control sequence (sh-ctrl), or sh-Snail and miR-21. Data represent means \pm S.D. n=3 independent experiment (each experiment contains 2 technical replicates).
- (F) Schema of the animal experiment in panel G.
- (G) Measurement of the volume of tumors formed by LLC1-shCtrl/LLC1-shSnail cells. 2×10^5 cells were inoculated to the subcutaneous region of C57BL/6 mice. Cisplatin (5 mg/kg/day) were given for 4 continuous days since the tumor reached 50mm³. The mice were sacrificed at the 15th day after cisplatin/PBS treatment. Tumor volumes were recorded. Data (n>2) were presented in mean \pm S.D.



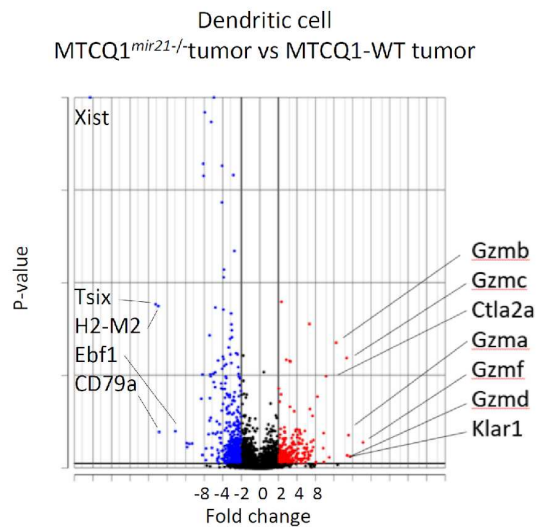
Supplementary figure 8. Analysis of the infiltrated immune cells in murine oral cancers by single cell RNA sequencing.

- (A) Schema of the experiment. 1×10^6 MTCQ-WT/MTCQ^{mir21^{-/-}} cells were inoculated to the subcutaneous region of the C57BL/6J mice for 2 weeks (n=3 for each group). Cisplatin 5mg/kg was given intraperitoneally on 14th day and the mice were sacrificed 72 h after cisplatin injection. The tumors were harvested and the CD45⁺ cells were isolated by magnetic beads for the droplet-based single cell RNA sequencing and subsequent analysis.
- (B) t-SNE plots of the immune cells expressing different markers (CD4, CD8a, CD11c, CD79a, F4/80, and Foxp3) in MTCQ1-WT and MTCQ1^{mir21^{-/-}}-formed tumors 3 days after cisplatin (5mg/kg) injection.
- (C) GO enrichment analysis of the biological pathways of the TAMs in other clusters versus cluster 2 (see Figure 6F for the TAM clustering).
- (D) A heatmap for showing the expression of the M1 macrophages-related genes (left) and M2 macrophages-related genes (right) in different clusters of macrophages. Red, upregulation; green, downregulation.

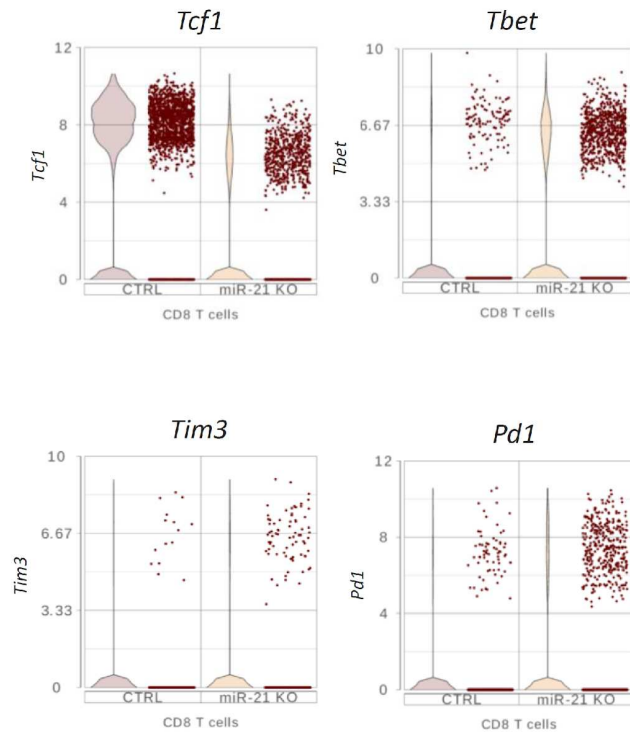
A



B

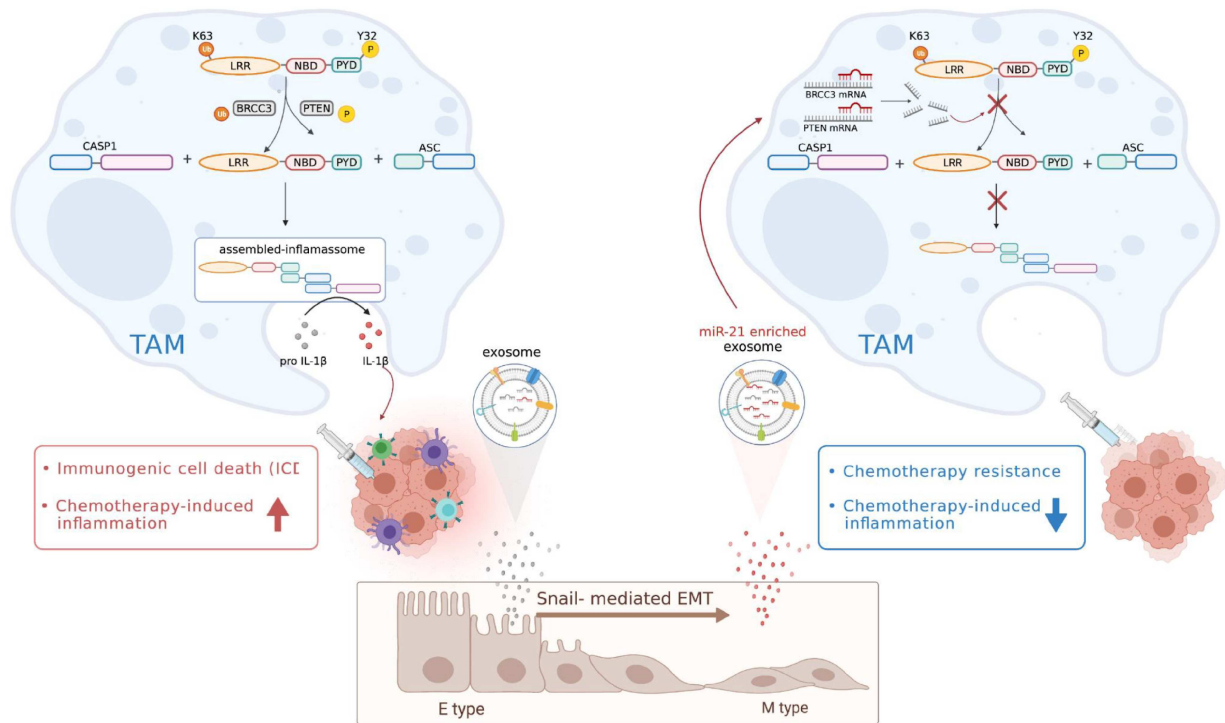


C



Supplementary figure 9. Single cell RNA sequencing analysis of the infiltrated immune cells in murine oral cancers.

- (A) Transcriptional trajectory of infiltrated macrophages and monocytes of the tumors.
- (B) Volcano plots of the differential expressed genes of the dendritic cells (classification by CIPR; see reference 28) from MTCQ^{mir21^{-/-}}-versus MTCQ1-WT-formed tumors. Red, upregulated genes; blue, downregulated genes.
- (C) Violin plots to show the expression of the exhausted T cell markers (*Tcf1*, *Tbet*, *Tim3*, *Pd1*) in CD8⁺ T cells of the MTCQ1-WT and MTCQ1^{mir21^{-/-}} tumors.



Supplementary figure 10. The schema for representing the NLRP3 inflammasome activity of macrophages regulated by the Snail-miR-21 axis of cancer cells via exosomal delivery of miR-21. Created with [BioRender.com](https://www.biorender.com).

Supplementary Table Legends

Supplementary Table 1. Characteristics of 9 TVGH HNSCC patients for multiplex immunofluorescent staining

Supplementary Table 2. Characteristics of the TVGH HNSCC patients for bulk RNA sequencing analysis (65 tumor tissues and 21 normal counterparts from 21 patients)

Supplementary Table 3. Characteristics of the TVGH HNSCC patients for RT-qPCR analysis (n=50)

Supplementary Table 4. Characteristics of the TVGH HNSCC patients for serum IL-1 β analysis (n=19)

Supplementary Table 5. Characteristics of the TVGH HNSCC patients for immunofluorescent staining-PLA co-localization analysis (n=5)

Supplementary Table 6. List of the inflammasome-related genes and EMT genes for Visium spatial transcriptomic analysis

Supplementary Table 7. microRNA sequence profile in FaDu exosomes versus SG exosomes

Supplementary Table 8. Cell counts of different immune cells of the single cell RNA sequencing experiment

Supplementary Table 9. Differential gene expression of TAMs from MTCQ1-WT- vs. MTCQ1^{mir21^{-/-}}-formed tumors

Supplementary Table 10. GO enrichment analysis of the TAMs from MTCQ1-WT- vs. MTCQ1^{mir21^{-/-}}-formed tumors

Supplementary Table 11. Cell counts of macrophage subclusters of the single cell RNA sequencing experiment

Supplementary Table 12. GO enrichment analysis of the TAM subcluster 2 vs other TAM subclusters

Supplementary Table 13. Differential gene expression of dendritic cells MTCQ1-WT- vs. MTCQ1^{mir21^{-/-}}-formed tumors

Supplementary Table 14. Antibodies, primers, plasmids, reagents, clinical samples, and other materials used in this study

Supplementary table 14. Antibodies, primers, plasmids, reagents, clinical samples, and other materials used in this study

| REAGENT or RESOURCE | SOURCE | IDENTIFIER |
|---|---|-------------|
| Antibodies | | |
| Anti-CD63 Antibody, clone RFAC4 | Merck KGaA, Burlington, MA | CBL553 |
| Anti-CD81 antibody | GeneTex, Inc, Irvine, CA | GTX101766 |
| Alix (3A9) Mouse mAb | Cell Signaling Technology, Inc, Danvers, MA | #2171 |
| Snail (L70G2) Mouse mAb, for WB | Cell Signaling Technology, Inc, Danvers, MA | #3895 |
| Snail polyclonal antibody, for IHC | Abnova Corporation, Taipei, Taiwan | PAB1924 |
| Monoclonal ANTI-FLAG® M2 antibody | Merck KGaA, Burlington, MA | F1804 |
| Purified anti-HA.11 Epitope Tag Antibody | BioLegend, Inc, San Diego, CA | 901502 |
| Anti-Caspase-1 antibody | Abcam plc, Cambridge, UK | ab17820 |
| IL-1 β Antibody (H-153) | Santa Cruz Biotechnology, Inc, Santa Cruz, CA | sc-7884 |
| Anti-IL-6 antibody [B-E8] | Abcam plc, Cambridge, UK | ab11449 |
| Human IL-8/CXCL8 Antibody | R&D Systems, Inc, Minneapolis, MN | AF-208-NA |
| Human CCL2/JE/MCP-1 Antibody | R&D Systems, Inc, Minneapolis, MN | AF-279-NA |
| Human CCL5/RANTES Antibody | R&D Systems, Inc, Minneapolis, MN | AF-278-NA |
| ASC Antibody (N-15), for WB and IP | Santa Cruz Biotechnology, Inc, Santa Cruz, CA | sc-22514-R |
| ASC/TMS1 Antibody, for PLA | Novus Biologicals, Centennial, CO | NBP1-78977 |
| anti-NLRP3/NALP3, mAb antibody (Cryo-2) | Adipogen Life Sciences, San Diego, CA | AG-20B-0014 |
| K63-linkage Specific Polyubiquitin (D7A11) Rabbit mAb | Cell Signaling Technology, Inc, Danvers, MA | #5621 |
| CD14 MicroBeads, human | Miltenyi Biotec, Bergisch Gladbach, Germany | 130-050-201 |
| IFN gamma Monoclonal Antibody (XMG1.2) | Thermo Fisher Scientific Inc, Waltham, MA | 17-7311 |
| CD8a Antibody, anti-mouse, PE | Miltenyi Biotec, Bergisch Gladbach, Germany | 130-102-595 |
| PE/Cyanine7 anti-mouse CD45 Antibody | BioLegend, Inc, San Diego, CA | 103114 |
| APC anti-mouse F4/80 Antibody | BioLegend, Inc, San Diego, CA | 123116 |
| PE/Cyanine7 Rat IgG2b, κ Isotype Ctrl Antibody | BioLegend, Inc, San Diego, CA | 400617 |

| | | |
|---|---|---------------------------------------|
| APC Rat IgG2a, κ Isotype Ctrl Antibody | BioLegend, Inc, San Diego, CA | 400511 |
| CD68 | Agilent Technologies, Inc, Santa Clara, CA | M0876 |
| Goat anti-Mouse IgG | Thermo Fisher Scientific Inc, Waltham, MA | F2761 |
| Anti-Actin Antibody | Thermo Fisher Scientific Inc, Waltham, MA | MAB1501 |
| GAPDH (14C10) Rabbit mAb | Cell Signaling Technology, Inc, Danvers, MA | #2118 |
| normal mouse IgG | Santa Cruz Biotechnology, Inc, Santa Cruz, CA | sc-2025 |
| BRCC3 (D5E5H) Rabbit mAb | Cell Signaling Technology, Inc, Danvers, MA | #18215 |
| PTEN (D4.3) XP® Rabbit mAb | Cell Signaling Technology, Inc, Danvers, MA | #9188 |
| Anti-CD9 antibody | Abcam plc, Cambridge, UK | ab92726 |
| Anti-CD81 antibody | GeneTex, Inc, Irvine, CA | GTX101766 |
| Anti-Calreticulin antibody | Abcam plc, Cambridge, UK | ab39897 |
| CD45 MicroBeads, mouse | Miltenyi Biotec, Bergisch Gladbach, Germany | 130-052-301 |
| PerCP anti-mouse F4/80 Antibody | BioLegend, Inc, San Diego, CA | 123126 |
| Gasdermin D (E8G3F) Rabbit mAb | Cell Signaling Technology, Inc, Danvers, MA | #97558 |
| A20/TNFAIP3 (D13H3) Rabbit mAb | Cell Signaling Technology, Inc, Danvers, MA | #5630 |
| CD4, for multiplex IHC | Thermo Fisher Scientific Inc, Waltham, MA | Clone: 4B12 |
| CD8a, for multiplex IHC | Thermo Fisher Scientific Inc, Waltham, MA | Clone: C8/144B |
| CD163, for multiplex IHC | Thermo Fisher Scientific Inc, Waltham, MA | Clone: 10D6 |
| CD68, for multiplex IHC | Abcam plc, Cambridge, UK | Clone: KPI |
| CD66b, for multiplex IHC | BD, Franklin Lakes, NJ | Clone: G10F5 |
| PanCK, for multiplex IHC | Abcam plc, Cambridge, UK | Clone: AE1/AE3+5D3 |
| Bacterial and Virus Strains | | |
| Stbl3 | Thermo Fisher Scientific Inc, Waltham, MA | C737303 |
| Biological Samples | | |
| 9 samples from HNSCC patients for multiplex immunofluorescent staining (Figure S1A, Table S1) | Taipei Veterans General Hospital | TVGH-IRB certificate No.2018-06-00 |

| | | |
|--|---|---|
| 44 tumor samples with 21 normal counterparts from 21 HNSCC patients for RNA-seq analysis (Figure 1B, Table S2) | Taipei Veterans General Hospital | TVGH-IRB certificate No.2017-05-013AC IBC |
| 50 samples from HNSCC patients for RT-qPCR (Figure 7B, Table S10) | Taipei Veterans General Hospital | TVGH-IRB certificate No. 2014-03-004AC |
| Serum and tissue samples from 19 HNSCC patients (Figure 7C-D, Table S11) | Taipei Veterans General Hospital | TVGH-IRB certificate No. 2014-03-004AC |
| 5 samples from 5 HNSCC patient for immunofluorescence and PLA (Figure 7E, Table S12) | Taipei Veterans General Hospital | TVGH-IRB certificate No. 2014-03-004AC |
| PBMC from healthy donors | Taipei Veterans General Hospital | TVGH-IRB certificate No. 2014-03-004AC |
| Chemicals, Peptides, and Recombinant Proteins | | |
| Nigericin sodium salt | Merck KGaA, Burlington, MA | N7143 |
| Phorbol 12-myristate 13-acetate (PMA) | Cayman Chemical, Ann Arbor, MI | 10008014 |
| Lipopolysaccharides (LPS) | Merck KGaA, Burlington, MA | L4391 |
| Cisplatin | Merck KGaA, Burlington, MA | PHR1624 |
| T-Pro NTR III | JF Ji-Feng Biotechnology, New Taipei County, Taiwan | JT97-N006M |
| Human IFN- γ | PeproTech, Inc, Cranbury, NJ | 300-02 |
| Murine Ifn- γ | PeproTech, Inc, Cranbury, NJ | 315-05 |
| Human GM-CSF | PeproTech, Inc, Cranbury, NJ | 300-03 |
| Murine Gm-csf | PeproTech, Inc, Cranbury, NJ | 315-03 |
| 7-AAD Staining Solution | Abcam plc, Cambridge, UK | ab228563 |
| SYTOX™ Green Nucleic Acid Stain | Thermo Fisher Scientific Inc, Waltham, MA | S7020 |
| Critical Commercial Assays | | |
| IL-1 beta Human Instant ELISA™ Kit | Thermo Fisher Scientific Inc, Waltham, MA | BMS224INST |
| Mouse Il-1 beta Instant ELISA™ Kit | Thermo Fisher Scientific Inc, Waltham, MA | BMS6002INST |
| TA Cloning™ Kit | Thermo Fisher Scientific Inc, Waltham, MA | K202020 |
| Duolink™ In Situ PLA® Probe Anti-Mouse PLUS | Merck KGaA, Burlington, MA | DUO92001 |
| Duolink™ In Situ PLA® Probe Anti-Rabbit MINUS | Merck KGaA, Burlington, MA | DUO92005 |
| Duolink™ In Situ Detection Reagents Red | Merck KGaA, Burlington, MA | DUO92008 |

| | | |
|--|---|---|
| FLICA 660 Caspase-1 Assay | ImmunoChemistry Technologies, LLC, Bloomington, MN | #9122 |
| Tumor Dissociation Kit, mouse | Miltenyi Biotec, Bergisch Gladbach, Germany | 130-096-730 |
| Dead Cell Removal Kit | Miltenyi Biotec, Bergisch Gladbach, Germany | 130-090-101 |
| Opal Polaris 7 Color IHC Detection Kits | Akoya Biosciences, Inc, Marlborough, MA | NEL861001KT |
| Deposited Data | | |
| TCGA HNSCC RNA sequence data | National cancer institute, Rockville, MD | https://www.cancer.gov/about-nci/organization/ccg/research/structural-genomics/tcga |
| TVGH RNA sequence data | This paper | GSE178537 |
| scRNA-seq of CD45+ cells of MTCQ1-WT/MTCQ1 ^{mir21-/-} - formed tumors | This paper | GSE172326 |
| small RNA sequencing of the cancer cell-secreted exosomes | This paper | GSE99474 |
| Visium spatial gene expression data | This paper | GSE181300 |
| Experimental Models: Cell Lines | | |
| Human: FaDu cells | ATCC, Manassas, VA | HTB-43 |
| Human: OECM1 cells | Dr. Kuo-Wei Chang's lab | Hung et al., 2014 |
| Human: THP-1 cells | ATCC, Manassas, VA | TIB-202 |
| Human: HEK 293T cells | ATCC, Manassas, VA | CRL-3216 |
| Mouse: MTC-Q1 | Dr. Kuo-Wei Chang's lab | (Chen et al., 2019) |
| Mouse: LLC1 | ATCC, Manassas, VA | CRL-1642 |
| Mouse: 4T1 | ATCC, Manassas, VA | CRL-2539 |
| Experimental Models: Organisms/Strains | | |
| Mouse: C57BL/6JNarl | National Laboratory Animal Center, Taipei, Taiwan | N/A |
| Mouse: BALB/cByJNarl | National Laboratory Animal Center, Taipei, Taiwan | N/A |
| Mouse: Nlrp3 ^{-/-} | Dr. Nien-Jung Chen's lab | N/A |
| Oligonucleotides | | |
| miR-21-5p agomir | Ribobio Corp, Guangzhou, China. | miR40000790-1-2 |
| agomir Negative Control | Ribobio Corp, Guangzhou, China. | miR04201-1-10 |
| Recombinant DNA | | |
| pCDH-CMV-MCS-EF1-puro vector | System Biosciences | CD710B-1 |
| pMD.G | RNA Technology Platform and Gene Manipulation Core of Academia Sinica, Taipei, Taiwan | C6-6-1 |

| | | |
|---|---|---|
| pCMVΔR8.91 | RNA Technology Platform and Gene Manipulation Core of Academia Sinica, Taipei, Taiwan | C6-6-1 |
| pMIR-REPORT | Thermo Fisher Scientific Inc, Waltham, MA | AM5795 |
| pRK5-HA-Ubiquitin-K63 | Addgene, Watertown, MA | #17606 |
| pLKO.1-scramble | RNA Technology Platform and Gene Manipulation Core of Academia Sinica, Taiwan | ASN0000000004 |
| pLKO.1-SNAI1 shRNA | RNA Technology Platform and Gene Manipulation Core of Academia Sinica, Taiwan | TRCN0000063818 |
| pLKO.1-mouse Snai1 shRNA | RNA Technology Platform and Gene Manipulation Core of Academia Sinica, Taiwan | TRCN0000234034 |
| pGreenPuro control lentivector (control for pmiRZip21) | System Biosciences, LLC, Palo Alto, CA | SI505A-1 |
| pmiRZip21 anti-miR-21 expression lentivector | System Biosciences, LLC, Palo Alto, CA | MZIP21-PA-1 |
| pcDNA3-Flag-NLRP3 | Dr. Szu-Ting Chen's lab | N/A |
| SgRNA/Cas9-MIR21-1: GTCTGATAAGCTACCCGACAAGG | Dr. Tsai-Yu Tzeng's lab | subcloned into PX459 by BbsI site. |
| SgRNA/Cas9-MIR21-2: TCATGGCAACACCAGTCGATTGG | Dr. Tsai-Yu Tzeng's lab | subcloned into PX459 by BbsI site. |
| SgRNA/Cas9 -mMIR21a-1: GTCTGATAAGCTATCCGACAAGG | Dr. Tsai-Yu Tzeng's lab | subcloned into PX459 by BbsI site. |
| SgRNA/Cas9-mMIR21a-2: TCATGGCAACAGCAGTCGATGGG | Dr. Tsai-Yu Tzeng's lab | subcloned into PX459 by BbsI site. |
| Software and Algorithms | | |
| ImageJ | Schneider et al., 2012 | https://imagej.nih.gov/ij/ |
| GraphPad Prism8 | GraphPad Software, San Diego, CA | https://www.graphpad.com/ |
| FV31S-SW | Olympus Corporation, Tokyo, Japan | https://www.olympus-global.com/ |
| Partek Flow | Partek, St. Louis, MO | https://www.partek.com/partek-flow/ |
| CIPR | N/A | (Ekiz et al., 2020) |
| DAVID Bioinformatics Resources 6.8 | N/A | (Huang da et al., 2009) |
| GSEA | N/A | (Subramanian et al., 2005) |

| Oligonucleotides | |
|-----------------------------------|--|
| Primers for reverse transcription | Sequence (5'-3') |
| hsa-mir-21 | GTCGTATCCAGTGCAGGGTCCGAGGTATTTCGACTGGATACGACTCAACA |
| hsa-mir-10a | GTCGTATCCAGTGCAGGGTCCGAGGTATTTCGACTGGATACGACCACAAA |
| hsa-mir-30a | GTCGTATCCAGTGCAGGGTCCGAGGTATTTCGACTGGATACGACCTTCCA |
| hsa-mir-30d | GTCGTATCCAGTGCAGGGTCCGAGGTATTTCGACTGGATACGACCTTCCA |
| hsa-let-7i | GTCGTATCCAGTGCAGGGTCCGAGGTATTTCGACTGGATACGACAACAGC |
| hsa-mir-182 | GTCGTATCCAGTGCAGGGTCCGAGGTATTTCGACTGGATACGACAGTGTG |
| hsa-mir-191 | GTCGTATCCAGTGCAGGGTCCGAGGTATTTCGACTGGATACGACCAGCTG |
| hsa-mir-205 | GTCGTATCCAGTGCAGGGTCCGAGGTATTTCGACTGGATACGACCAGACT |
| hsa-mir-1246 | GTCGTATCCAGTGCAGGGTCCGAGGTATTTCGACTGGATACGACCCTGCT |
| hsa-mir-4792 | GTCGTATCCAGTGCAGGGTCCGAGGTATTTCGACTGGATACGACGCCAGC |
| qPCR primers | Sequence (5'-3') |
| <i>BRCC3</i> -F | TTCCCGATAGTGACATGAGG |
| <i>BRCC3</i> -R | CAGGCCCAAAAGAGTTCAGA |
| miR-21-F | GCCGCTTAGCTTATCAGACTGA |
| miR-21-R | GTGCAGGGTCCGAGGT |
| Ifng-F (m) | CGGCACAGTCATTGAAAGCCTA |
| Ifng-R (m) | GTTGCTGATGGCCTGATTGTC |
| <i>CXCL10</i> -F | GCAGGTACAGCGTACGGTTC |
| <i>CXCL10</i> -R | CAGCAGAGGAACCTCCAGTC |
| <i>CXCL9</i> -F | CCTTAAACAATTTGCCCAA |
| <i>CXCL9</i> -R | TCACATCTGCTGAATCTGGG |
| <i>IFNG</i> -F | TGTATTGCTTTGCGTTGGAC |
| <i>IFNG</i> -R | TGACCAGAGCATCCAAAAGA |
| <i>GAPDH</i> -F | AAGGTCGGAGTCAACGGATTTG |
| <i>GAPDH</i> -R | CCATGGGTGGAATCATATTGGAA |
| <i>U6</i> -F | CTCGCTTCGGCAGCAC |
| <i>U6</i> -R | AACGCTTCACGAATTTGCG |
| <i>ASC</i> -F | CAGGACCTTCCCGTACAGAG |
| <i>ASC</i> -R | CAGGACCTTCCCGTACAGAG |
| <i>NLRP3</i> -F | ACGTAAGGCCAGAATTCACC |
| <i>NLRP3</i> -R | GAATGCCTTGGGAGACTCAG |
| <i>PDCD4</i> -F | TCCTCAGTCCCAGCATTTC |
| <i>PDCD4</i> -R | TGCAAGCGAAATTAAGGGAA |
| miR-205-F | GCCGCTTCCTTCATTCCACCGG |
| miR-205-R | GTGCAGGGTCCGAGGT |
| miR-30a-F | GCCGCTTGTAACATCCTCGAC |
| miR-30a-R | GTGCAGGGTCCGAGGT |
| miR-182-F | GCCGCTTTTGGCAATGGTAGAACT |

| | |
|---------------------|--------------------------|
| miR-182-R | GTGCAGGGTCCGAGGT |
| miR-30d-F | GCCGCTTGTAACATCCCCGAC |
| miR-30d-R | GTGCAGGGTCCGAGGT |
| miR-4792-F | GCCGCTCGGTGAGCGCTC |
| miR-4702-R | GTGCAGGGTCCGAGGT |
| let-7i-F | GCCGCTTGAGGTAGTAGTTTGT |
| let-7i-R | GTGCAGGGTCCGAGGT |
| miR-10a-F | GCCGCTTACCCTGTAGATCCGAA |
| miR-10a-R | GTGCAGGGTCCGAGGT |
| miR-191-F | GCCGCTCAACGGAATCCCAAAG |
| miR-191-R | GTGCAGGGTCCGAGGT |
| miR-1246-F | GCCGCTAATGGATTTTGG |
| miR-1246-R | GTGCAGGGTCCGAGGT |
| <i>Gapdh</i> -F (m) | CATGGCCTTCCGTGTTTCCTA |
| <i>Gapdh</i> -R (m) | TGTCATCATACTTGGCAGGTTTCT |
| <i>Snail</i> -F (m) | CACACGCGTGCCTTGTGTCT |
| <i>Snail</i> -F (m) | GGTCAGCAAAAGCACGGTT |
| pri-miR-21-F | AATCCTGCCTGACTGTCCG |
| pri-miR-21-R | ATGTCAGACAGCCCATCGAC |